# An Open-Source Deep Learning-Based GUI Toolbox For Automated Auditory Brainstem Response Analyses (ABRA)

Abhijeeth Erra<sup>1\*</sup>, Jeffrey Chen<sup>1\*</sup>, Elena Chrysostomou<sup>3</sup>, Shannon Barret<sup>3</sup>, Cayla Miller<sup>3</sup>, Yasmin M. Kassim<sup>3</sup>, Rick A. Friedman<sup>4</sup>, Federico Ceriani<sup>5,6</sup>, Walter Marcotti<sup>5,6</sup>, Cody Carroll<sup>1,2</sup>, Uri Manor<sup>3,4,7,°</sup>

\*denotes equal contribution

#### **Abstract**

In this paper, we introduce a new, open-source software developed in Python for analyzing Auditory Brainstem Response (ABR) waveforms. ABRs are a far-field recording of synchronous neural activity generated by the auditory fibers in the ear in response to sound, and used to study acoustic neural information traveling along the ascending auditory pathway. Common ABR data analysis practices are subject to human interpretation and are labor-intensive, requiring manual annotations and visual estimation of hearing thresholds. The proposed new Auditory Brainstem Response Analyzer (ABRA) software is designed to facilitate the analysis of ABRs by supporting batch data import/export, waveform visualization, and statistical analysis. Techniques implemented in this software include algorithmic peak finding, threshold estimation, latency estimation, time warping for curve alignment, and 3D plotting of ABR waveforms over stimulus frequencies and decibels. The excellent performance on a large dataset of ABR collected from three labs in the field of hearing research that use different experimental recording settings illustrates the efficacy, flexibility, and wide utility of ABRA.

<sup>&</sup>lt;sup>1</sup> Data Institute, University of San Francisco, San Francisco, CA

<sup>&</sup>lt;sup>2</sup>Dept. of Mathematics and Statistics, University of San Francisco, San Francisco, CA

<sup>&</sup>lt;sup>3</sup>Dept. of Cell & Developmental Biology, University of California San Diego, La Jolla, CA,

<sup>&</sup>lt;sup>4</sup>Dept. of Otolaryngology, University of California San Diego, La Jolla, CA

<sup>&</sup>lt;sup>5</sup>Dept. of Biomedical Science, University of Sheffield, Sheffield, S10 2TN, UK.

<sup>&</sup>lt;sup>6</sup>Neuroscience Institute, University of Sheffield, Sheffield, S10 2TN, UK.

<sup>&</sup>lt;sup>7</sup>Halıcıoğlu Data Science Institute, University of California San Diego, La Jolla, CA

<sup>°</sup>Corresponding author: uri@ucsd.edu

# Introduction

Auditory brainstem response (ABR) recordings provide an objective measurement of electrical activity along the ascending auditory neural pathway, starting from the afferent fibers

innervating the inner hair cells in the cochlea through the brainstem nuclei (Eggermont 2019; Kim et al. 2022; Burkard and Don 2012; Ingham et al. 2011; Møller and Jannetta 1985; Xie et al. 2018). ABRs are widely used in auditory research to study acoustic neural information transmission and to diagnose and distinguish different forms of hearing loss and synaptopathy in animal models of human otologic and neurologic conditions (Sininger 1993; Burkard and Sims 2001; Fernandez et al., 2015; Bramhall et al., 2018; Bao et al., 2022; Young, Cornejo, and Spinner 2023). In mice, ABR waveforms consist of five characteristic peaks (Figure 1), each approximately corresponding to the sound-induced electrical signal traveling through the different structures along the auditory pathway (Figure 1, Rüttiger et. al. 2017, Melcher et al. 1996, Henry 1979, Land et al. 2016).

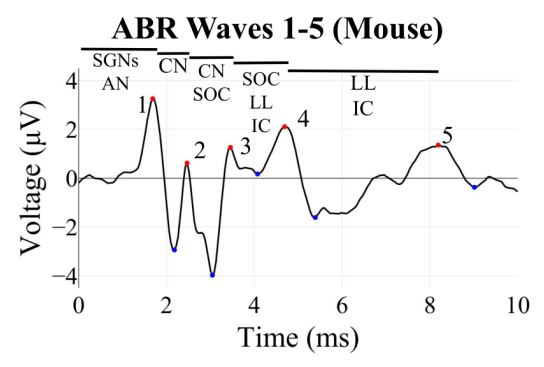


Figure 1: Example of an ABR waveform recorded from a mouse showing its characteristic features or waves. Wave 1 is generated by the spiral ganglion neurons (SGNs) and auditory nerve (AN), Wave 2 by the cochlear nucleus (CN), Wave 3 by the CN and superior olivary complex (SOC), Wave 4 by the SOC, lateral lemniscus (LL) and inferior colliculus (IC), and Wave 5 by the LL and IC (Rüttiger et. al. 2017, Melcher et al. 1996, Henry 1979, Land et al. 2016). Peaks of these waves are denoted by red dots, and troughs with blue dots.

A key goal of ABR threshold analysis in mice is to generate quantitative measures of hearing function, defined as the minimum sound intensity (in decibels) at a given frequency that elicits a repeatable neural response. Traditionally, threshold identification is performed by visually inspecting waveforms at decreasing sound intensities until a waveform is no longer distinguishable from baseline noise. ABR thresholds in anesthetized mice are typically ~10dB higher than behavioral perceptual responses in awake mice (Radziwon et al. 2009). While pragmatic, this method is time-consuming for larger studies and prone to inconsistency and bias between labs and examiners (Suthakar and Liberman 2019, Schrode 2022). To address these limitations, heuristic and machine learning computational approaches have been explored for automated ABR analysis. Supervised learning models (i.e. models which learn from data with ground truth labels) like convolutional neural networks (CNN), gradient boosting machines, and others have been used to accurately analyze suprathreshold ABR waveforms (Wimalarathna et al. 2021, McKearney and MacKinnon 2019, Kamerer et al. 2020) and to assess the degree of synaptopathy in humans (Buran et al. 2022). The utility of unsupervised learning models (i.e. models which learn from data without ground truth labels) for ABR analysis remains relatively unexplored to date. Assuming a similar amount of training data, unsupervised models often have a harder task than supervised models since they cannot learn from true labels. However,

application of unsupervised methods often comes with reduced human labor requirements, since they do not require manually annotated ground truth data from which to learn.

In this paper, we introduce the Auditory Brainstem Response Analyzer (ABRA), a novel open-source software that implements a collection of supervised and unsupervised machine learning models trained on a diverse range of mouse ABR datasets from multiple labs for comprehensive and maximally generalizable mouse ABR analysis. ABRA is a user-friendly, browser-based application that supports batch data import/export, waveform visualization, automated peak detection, threshold estimation, latency quantification, time warping for curve alignment, and interactive 2D/3D plotting. By integrating these diverse functionalities into a unified platform, ABRA aims to streamline ABR data processing and analysis, reduce manual labor, and facilitate standardization and reproducibility across labs. We demonstrate ABRA's flexibility and generalizability by benchmarking its performance on ABR datasets collected from three different hearing research labs using distinct experimental protocols and recording settings.

#### **Methods**

#### **Data Collection**

To test for the generalizability and flexibility of developed open-source ABR software, we used three distinct datasets from different labs to train and evaluate ABRA's models (**Tables 1 - 2**). Each dataset used in the analysis was collected under unique experimental conditions and protocols. All three labs used a similar overarching methodology, including the use of anesthesia, electrodes, and sound decibel (dB) ranges. However, there were also differences in the specifics of these procedures, as outlined in **Table 1**. These differences underscore the flexibility of ABRA in accommodating diverse experimental setups and protocols. Further details on data collection conditions are available in the Supplementary Information.

Methods	Lab A	Lab B	Lab C
Anesthesia	Ketamine (90 mg/kg) + Xylazine (10 mg/kg)	Ketamine (100 mg/kg) + Xylazine (10 mg/kg)	Ketamine (100 mg/kg) + Xylazine (10 mg/kg)
Environme nt	Soundproof chamber, heating pad (37°C)  Soundproof chamber, heating pad (37°C)  Soundproof chamber, heating pad (37°C)  Soundproof chamber, heating pad (37°C)		Soundproof chamber, heating pad (37°C)
Electrode Placement	Subcutaneous recording electrode at vertex, reference behind right pinna, ground on left leg	Subdermal electrodes behind pinna (reference and ground), vertex (active)	Needle electrodes: vertex to ipsilateral pinna (recording), ground near tail
Sound Stimuli	5-ms tone pips (0.5 ms cos2 risefall), 21/sec	5-ms pips (1.0-ms rise-fall with cos2 onset envelope), 42.6/sec	5-ms pips (0.5-ms rise-fall with cos2 onset envelope), 30/sec
Recording	Filtered (300 Hz - 3 kHz), averaged using BioSigRZ software, 512 responses averaged	Customized software (Ingham et al., 2011), RZ6 auditory processor, 256 responses averaged	Amplified (10,000X), filtered (100 Hz - 3 kHz), averaged with A-D board in LabVIEW system, 1024 responses averaged

Sound Intensity	Decreased from 90 dB SPL to 10/20 dB SPL in 5 dB steps	0-95 dB SPL in 5 dB steps	Raised from ~10 dB below threshold to 80 dB SPL in 5 dB steps
Speaker distance	Open-field - 10 cm from ear	Open-field - 10 cm from ear	Closed-field - ~3 cm from the eardrum
Mouse age/strains used	3-month SAMP8 (Senescence- Accelerated Mouse-Prone 8) (Takeda et al. 1981)	1-month C57Bl/6N with and without corrected CDH23	7-week C57Bl/6J

**Table 1: Summary of the experimental recording conditions used by the three labs.** The datasets are described in the following order: Anesthesia, Preparation, Electrode Placement, Sound Stimuli, Recording, Sound Intensity, and Distance of the Speaker. The specific methods employed by each lab—Manor Lab (Lab A), Marcotti Lab (Lab B), Liberman Lab (Lab C)—are detailed in the supplementary information section.

Lab/Model	Peak Detection		Automatic Thresholding		
	Training Data	Test Data	Training Data	Test Data	ABRA vs. EPL-ABR
Lab A	40 mice (286 ABRs)	34 mice (72 ABRs)	65 mice (5,419 ABRs)	16 mice (2,031 ABRs)	-
Lab B	4 mice (327 ABRs)	4 mice (82 ABRs)	83 mice (12,948 ABRs)	21 mice (3,276 ABRs)	-
Lab C	-	-	29 mice (319 ABRs)	7 mice (77 ABRs)	27 mice (292 ABRs)
Total [Relevant Figures & Tables]	44 mice (613 ABRs) [Fig. 3]	38 mice (154 ABRs) [Fig. 6; Table 3]	177 mice (18,686 ABRs) [Fig. 4]	44 mice (5,384 ABRs) [Figs. 8-10; Tables 4, 5]	27 mice (292 ABRs) [Table 6]

**Table 2: Breakdown of mouse and ABR waveform data by lab, model, and train and test splits.** Figures and Tables relevant to a given dataset are enumerated in brackets in the last row.

#### The ABRA Graphical User Interface

The proposed Auditory Brainstem Response Analyzer (ABRA) software was built to facilitate the examination and analysis of ABR waveforms. ABRA was developed in Python using the Streamlit framework ("Streamlit" n.d.) and provides an interactive platform for researchers to visualize ABR data. The app is hosted at <a href="https://ucsdabranalysis.streamlit.app/">https://ucsdabranalysis.streamlit.app/</a> and all documentation can be found on our Github: <a href="https://github.com/ucsdmanorlab/abranalysis">https://github.com/ucsdmanorlab/abranalysis</a>. ABRA allows users to import multiple ABR data files stored in either .arf or .csv files obtained from BioSigRZ software from Tucker Davis Technologies (TDT). Upon import, the data is preprocessed to extract frequency, dB level, and the waveform data itself.

At its simplest functionality, ABRA allows the user to select which frequencies and decibel levels they wish to examine. The ABR plots are shown through the Plotly framework in Python

and can be downloaded as .png files. ABRA displays metrics under the plots related to the displayed waveforms, including Wave 1 amplitude, and latency to the first peak. These metrics can be downloaded into a .csv file. ABRA also allows the user to view all the waveforms for a single frequency, highlights the automatically detected peaks and troughs, and automates thresholding so that analysis can be performed more efficiently (**Figure 2**).

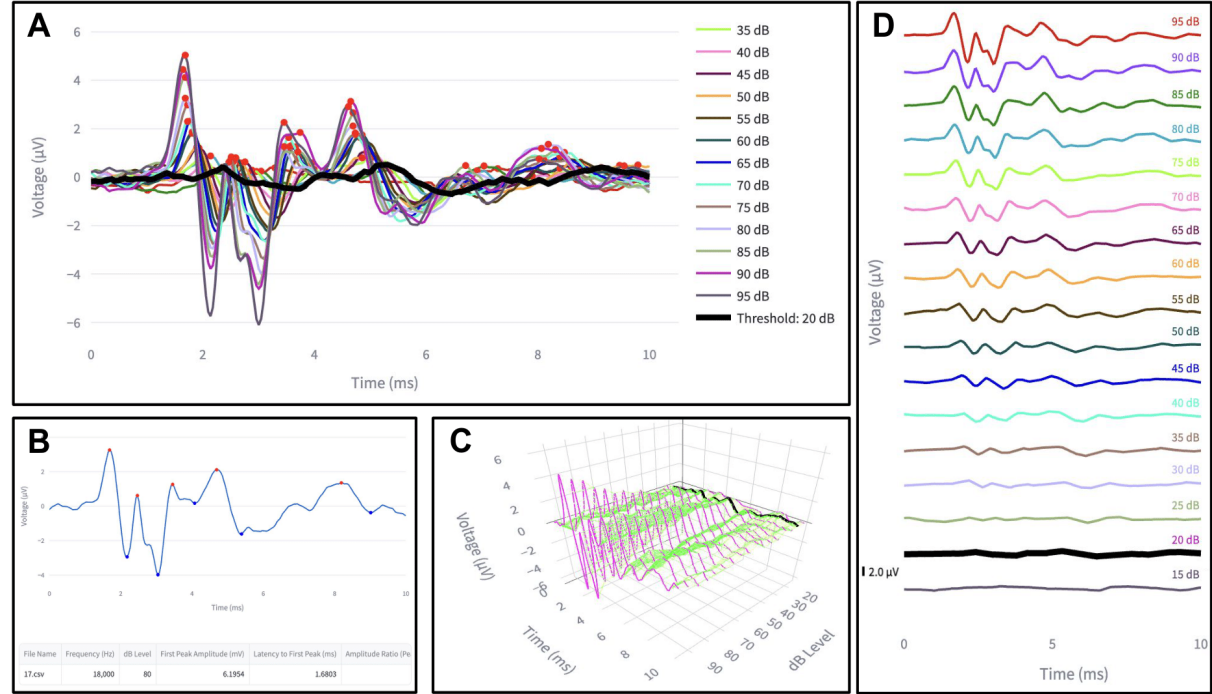
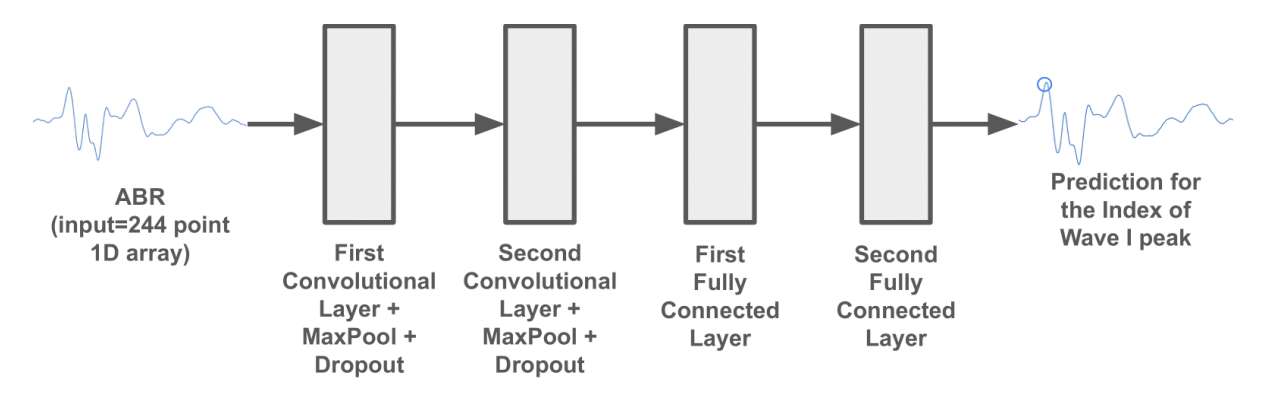


Figure 2: Screenshots from the ABRA app highlighting the different functionalities of ABRA (A) visualizing several ABR waveforms from one 1 mo male C57Bl/6N mouse across different togglable dBs at 18 kHz with predicted peak locations (red points) and predicted threshold (thick black line). (B) plotting a single ABR waveform at a specific sound frequency and intensity (dB SPL) with peaks and troughs labeled. (C) 3D plotting of all ABR waveforms at a given frequency with the predicted threshold (20dB) highlighted in black (can be rotated in the app). (D) stacks of ABR waveforms as a function of increasing dB SPL from the same frequency with the predicted threshold (20 dB) highlighted in black.

For those seeking a comprehensive view of the variations in the waveform over several dB levels at the same frequency for thresholding, ABRA provides the option to implement time warping which registers the peaks of the waveforms of multiple dBs in response to the same frequency of stimulation (see **Figure 5**). The app also provides a 3D surface plot of waveforms which is interactive and allows the user to view the series of ABR waveforms as cross-sections of the ABR voltage surface over the decibel and time domains. ABRA's different functionalities can provide the user the tools to visually threshold for themselves and compare their threshold with our model's prediction. ABRA also allows users to conduct these analyses for multiple data files in batches at the same time.

#### **ABRA Peak Detection**

ABRA incorporates a two-step peak finding algorithm that leverages Pytorch's deep learning library and the Scikit-learn library. The first step involves deploying a pre-trained Convolutional Neural Network (CNN) to retrieve a prediction for the location of the Wave 1 peak. We had 767 ABRs with ground truth labeled Wave 1 latencies and amplitudes (358 ABR waveforms from Lab A, 40 mice; 409 ABR waveforms from Lab B, 4 mice). We included 409 ABRs from Lab B to have a diversity of ABRs so that the model can be more thoroughly generalizable. Before training the CNN, the dataset was split into two sets with 80% of data from each lab going into the training set and 20% of data from each lab going into the testing set. The CNN was trained on 613 ABRs (286 ABRs from Lab A, 40 mice; 327 ABRs from Lab B, 4 mice) of length 244 (representing 10 ms) labeled with ground truth data related to the Wave 1 peak. The CNN optimizes squared error loss for the regression task which returns a prediction for the Wave 1 peak timepoint. A sparse representation of the network architecture is shown in **Figure 3**.



**Figure 3: Model architecture for Wave 1 Peak Finding Algorithm.** The ABR waveform recorded over 10 ms is input into two sequential layers of Convolution, Maxpool, and Dropout. The dimensionality of the output is reduced through two consecutive fully-connected layers which returns the prediction of the time point of the Wave 1 peak.

The CNN's prediction of the Wave 1 peak time point serves as a reasonable initial estimate but ABRA further performs some fine-tuning in order to ensure that it is not sitting at a point neighboring the peak. To retrieve the correct point of the peak of Wave 1, a second fine-tuning step was implemented as follows. First, the ABR was smoothed using Gaussian smoothing to attenuate or remove nuisance peaks to identify peak indices. Then the *find\_peaks* method from Scikit-learn was used to identify the remaining Wave 2-5 peak/trough locations and voltages by searching for all local maxima and minima by simple comparison of neighboring values of the wave starting from the CNN predicted Wave 1 peak index. Afterwards, the unsmoothed waveforms are utilized to quantify the amplitudes at the previously identified indices. The parameters for these methods were optimized using ground truth Wave 1 latency from 154 ABR waveforms (72 ABR waveforms from Lab A, 34 mice; and 82 ABR waveforms from Lab B, 4 mice) and ground truth Wave 4 amplitude from 211 labeled ABRs from Lab A. These parameters include the following:

- a. Window size for the start point for the smoothed waveform being inputted into the find peaks function (optimized to 0.3689 ms before the CNN prediction for Wave 1 peak).
- b. Time between peaks such that the correct peaks are identified (optimized to 0.7377 ms).
- c. Bandwidth parameter for the Gaussian smoothing step was set to  $\sigma = 1.0$ .
- d. Time between troughs such that the correct troughs are identified (optimized to 0.5738 ms).

### **Supervised Threshold Estimation with ABRA**

The threshold estimation method used a binary machine learning classifier to identify individual ABR waveforms as either above or below threshold. Once individual waveforms were identified, the hearing threshold for a given frequency was determined as the quietest stimulus level (in dB SPL) for which a subject's ABR waveform suggested a hearing response (i.e. was above threshold). Three candidate supervised binary classifiers were trained and evaluated: A CNN, an XGBoost classifier, and a Logistic Regression Classifier.

The dataset comprised 23,352 ABR waves from 221 mice (Lab A = 48 mice; Lab B = 104 mice; Lab C = 36 mice), with each wave characterized by its frequency, decibel level, and amplitudes at 244 uniformly distributed sampling points over a 10 ms time window. ABRs not initially sampled at 244 samples per 10 ms were resampled using linear interpolation. The ABRs were grouped by subject and frequency, then 80% of these groups were randomly allocated for training (Lab A = 34 mice; Lab B = 83 mice; Lab C = 27 mice) and the remaining 20% were designated for testing (Lab A = 14 mice; Lab B = 21 mice; Lab C = 9 mice). This method ensures a representative distribution of ABRs from various subjects and frequencies across the training and testing sets. Accordingly, the training input matrix had dimensions of 18,686 x 246, where 18,686 is the total number of training samples and 246 is the number of features, including 244 voltage recordings for each ABR, the decibel level, and the frequency of the stimulus.

For the Logistic Regression Classifier and XGBoost Classifier, time warping was used on the ABR trajectories as an additional preprocessing step to align waveform features such as peaks and troughs (see section below: **ABR Curve Alignment with Time Warping**). For the CNN, no additional preprocessing steps were used. The architecture of the CNN is described in **Figure 4**.

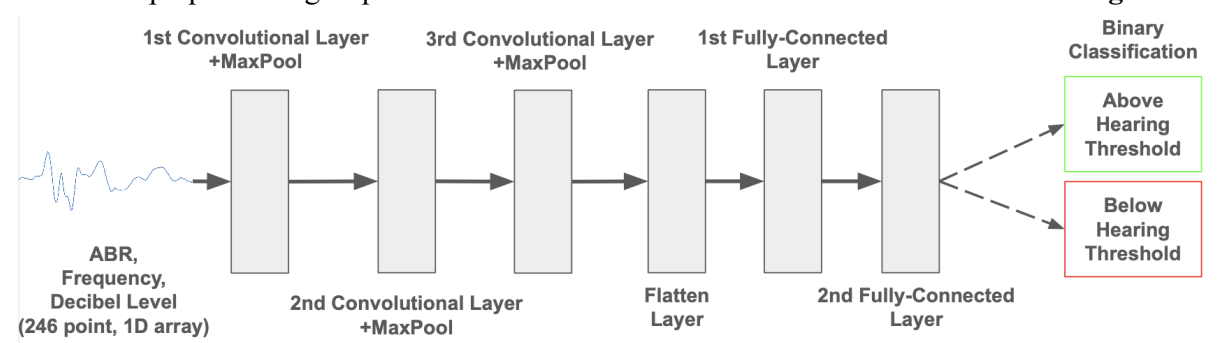


**Figure 4:** Model architecture for CNN ABR Classifier. The ABR waveform recorded over 10 ms and its frequency and decibel level are input into three sequential layers of convolution and max pooling. The dimensionality of the output is reduced through two consecutive fully-connected layers before returning the classification.

# **ABR Curve Alignment with Time Warping**

As previously discussed, ABRs from mice often exhibit a characteristic structure with 5 distinct peaks (**Figure 1**). However, a common challenge in analyzing these ABR waveforms is the non-uniform latency across different frequencies and decibel levels. This variability in latency can distort the time-based comparison of these responses, as the peaks do not occur at the same time instances across different ABRs. To address this, we provide an option to employ time warping to align these ABRs, which standardizes the position of peaks and other salient features of the ABRs across time. This alignment serves dual purposes. First, it decouples amplitude and phase variation, facilitating the visual comparison of amplitudes of ABR waveforms. Second, the encoding of time alignment parameters into individual-specific warping functions provides the option of incorporating these features into machine learning models, which in some cases improves the models' performance and predictive power. It is important to emphasize that the optional time warping as a preprocessing step should only be used when analyzing amplitude, but not latency variability.

To conduct the time warping step, we used the *fdasrsf* package in Python (Tucker 2020). This package implements elastic time warping, a method that allows for alignment of key signals in waveforms. This technique is particularly useful in our case, as it allows us to align the ABRs despite the non-uniform latency across different frequencies and decibel levels.

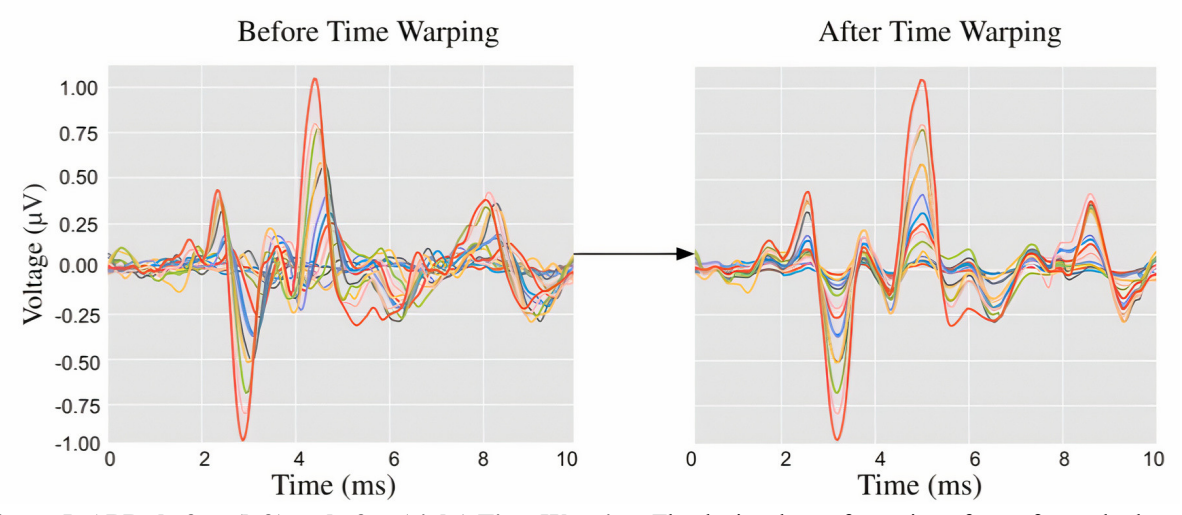


**Figure 5: ABRs before (left) and after (right) Time Warping.** The depicted transformation of waveforms, both before and after applying elastic time warping using the *fdasrsf* package (Tucker 2020), illustrates clear registration of waveform features. Associated with each waveform is also an estimated time warping function which is useful in quantifying changes between the original unaligned latencies to the aligned latencies for all wave peaks and troughs.

# **Unsupervised Threshold Estimation**

ABRA also provides an optional method to implement an unsupervised ABR threshold estimation, which uses ABR waveforms at a specific frequency across multiple dB levels. Following the optional time alignment of waveforms (see above section: **ABR Curve Alignment with Time Warping**), Functional Principal Component Analysis (FPCA) (Kleffe 1973) is used to identify and quantify what an eigenanalysis determines to be the most

significant patterns of variation in the ABR waveforms (e.g. averages and contrasts in wave peaks, troughs, and amplitudes, etc.). The waveforms are then projected onto their first and second principal components (PCs). This projection serves to reduce dimension, separate signal from noise, and cluster waveforms with similar salient ABR features, thereby simplifying the high-dimensional waveform data into a simple 2-dimensional representation. Only the first two PCs were used because they captured 95% of the variance in a set of typical ABRs, which indicates most of the signal can be represented using just these two components. Truncating at two components also discards later components which tend to be associated with noise.

Finally, ABRA employs a k-means clustering algorithm with 2 clusters on the projected data. The underlying assumption is that ABR waveforms above hearing threshold have higher principal component scores and will be clustered together, while the ABR waveforms below hearing threshold will form a separate cluster of near-zero principal component scores. This unsupervised approach allows users to identify natural groupings in the data without any prior assumptions about the number or characteristics of these groups.

#### Results

# **Peak Amplitude and Latency Estimation**

To benchmark ABRA's performance in peak amplitude and latency estimation, we fed a test set of 154 ABRs with human-labeled "ground truth" Wave 1 amplitude and latency values from Lab A (72 waveforms from 34 mice) and Lab B (82 waveforms from 4 mice) into ABRA. The ground truth values for Lab A data were obtained by using visual examination from two observers, while the ground truth values for Lab B data were obtained from manual labeling using custom software. Though it is possible to make manual adjustments to ABRA, we compare here only the absolute differences resulting from the automated (i.e. unadjusted) estimates generated from ABRA vs their corresponding human-labeled ground truth values in order to fairly assess its underlying model.

For each ABR waveform in the sample, let  $\tau_i^{(GT)}$  denote the corresponding ground truth latency and let  $a_i^{(GT)}$  denote the corresponding ground truth amplitude, with waveforms indexed by  $i=1,\ldots,n$ . Then, let  $\tau_i^{(ABRA)}$  denote the Wave 1 latency estimates generated by each software; similarly let  $a_i^{(ABRA)}$  denote ABRA's generated Wave 1 amplitude estimates.

Errors are then defined as the differences between a given software's estimate and the ground truth value. We define errors for Wave 1 latencies and amplitudes, respectively, as follows:

$$e_{\tau,i} = \tau_i^{(ABRA)} - \tau_i^{(GT)}, \quad i = 1, ..., n, and$$
  $e_{a,i} = a_i^{(ABRA)} - a_i^{(GT)}, \quad i = 1, ..., n.$ 

Side-by-side swarmplots of the distributions for error are shown for latency and amplitudes in **Figure 6A** and **6B**, respectively; summary statistics for errors are displayed in **Table 3**.

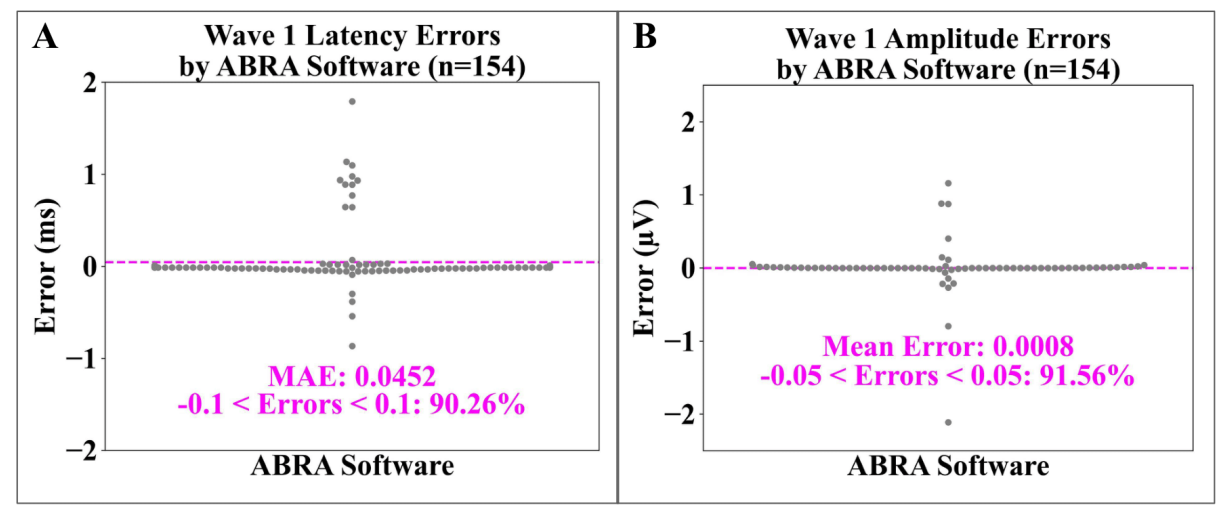


Figure 6: Swarmplots displaying spreads of error for detected Wave 1 Latency (A) and Amplitude (B) vs. ground truth for each software. Testing failed to find evidence that mean absolute errors were significantly greater than zero for both Wave 1 Latency and Amplitude estimates. 90.26% of all ABRA-generated estimates of Wave 1 Latency were within 0.1ms of the corresponding true human-labeled latency; 91.56% of all ABRA-generated Wave 1 amplitude were within 0.05  $\mu$ V of the corresponding true human-labeled peak amplitude. n = 154 represents the number of ABRs tested. Related statistics are listed in **Table 3.** 

Testing whether the centers of these distributions differed from zero showed that the average Wave 1 Latency errors produced by ABRA did not detect a significant deviation from zero ( $\underline{e}_{\tau} = 0.0452$ , SE = 0.0230, p = 0.0512) which suggests that ABRA is on average closely aligned with the human-labeled ground truth latencies. In a parallel comparison for amplitude estimates, hypothesis testing on the Wave 1 amplitude error distributions found that the average Wave 1 Amplitude error produced by ABRA did not deviate significantly from zero ( $\underline{e}_a = -0.015$ , SE = 0.0192, p = 0.9357) which suggests that ABRA amplitude estimates are on average closely aligned with the human-labeled ground truth amplitudes.

	Wave 1 Latency	Wave 1 Amplitude
Mean Difference (± S.E.M.)	ABRA vs. Ground Truth (ms)	ABRA vs. Ground Truth $(\mu V)$
Lab A (n <sub>waveforms</sub> =72, n <sub>mice</sub> =34)	0.0978 (±0.0467)	0.0008 (±0.0405)
Lab B (n <sub>waveforms</sub> =84, n <sub>mice</sub> =4)	-0.0010 (±0.0117)	$-0.0036 \ (\pm \ 0.0071)$
Overall Test Set	0.0452 (±0.0230)	-0.0015 (±0.0192)

Table 3 (related to Figure 6): Table showing the Mean Error Difference and their Standard Errors between ABRA-detected Wave 1 Latency and Amplitude and corresponding ground truth values detected by human reviewers. Testing failed to find evidence that mean error differences were significant for both Wave 1 Latency and Amplitude estimates. The peak finding method seems to be better for Wave 1 estimates in Lab B data (84 ABRs), but overall (154 ABRs) the errors are very low.

These comparisons show that ABRA-generated estimates generally agree with human-labeled ground truth latency and amplitude estimates, and when adjustments are needed they are small in magnitude. **Figure 7** displays a few visual examples of how errors from the ABRA software may

arise, with the most common source of errors arising from ABRs with very low signal-to-noise ratios (SNR).

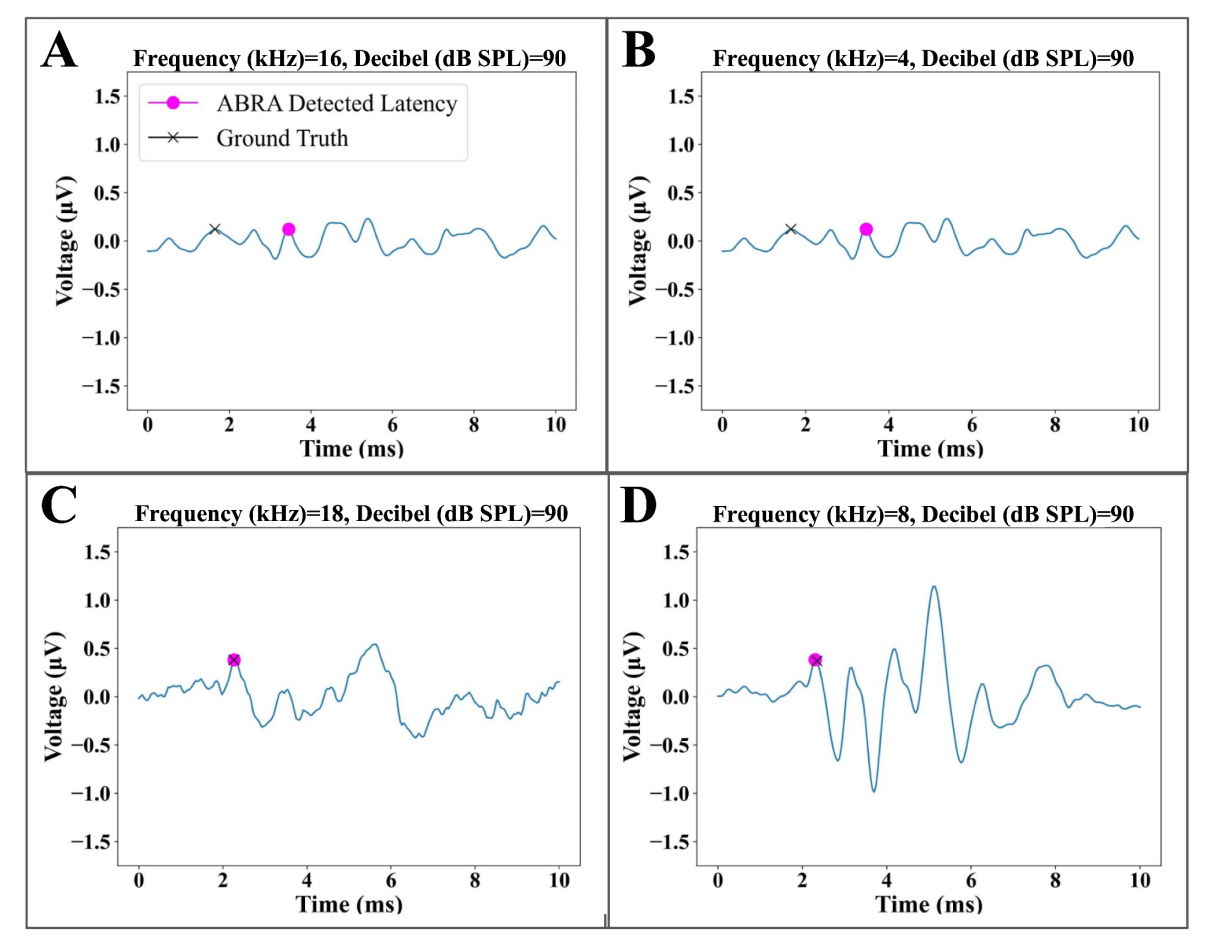


**Figure 7: Examples of error cases in peak detection. (A)** and **(B)** display examples of multiple peaks that may be identified as Wave 1 by different softwares and different sets of eyes, which are more difficult for ABRA to correctly detect. **(C)** and **(D)** are examples of ABR waveforms with larger signal to noise ratios for which ABRA matches the ground truth.

#### **ABR Classification and Threshold Estimation Results**

The performance of our ABR classifiers for threshold detection was assessed on the testing set of 5,384 ABR waveforms. Performance metrics are shown in **Figure 8** and a pairwise comparison for significance is provided in **Table 4**. As a simple and interpretable model, logistic regression was used as a baseline for the binary classification task. Despite its simplicity, it achieved an accuracy of 85.56%, a True Positive Rate (TPR), sometimes referred to as recall or sensitivity, of 90.27%, and an Area Under the Receiver Operating Characteristic Curve (AUROC) of 0.84. However, its performance was significantly outperformed by both the CNN and XGBoost models. The CNN model demonstrates superior performance in terms of accuracy (95.08%) and TPR (95.36%). These metrics surpass those of both the XGBoost and the baseline Logistic

Regression models, indicating the CNN's enhanced ability in correctly identifying ABR thresholds. However, it is noteworthy that the XGBoost model exhibits a slightly lower False Positive Rate (FPR) of 5.10%, compared to the CNN model's 5.49%. This suggests that the XGBoost model may be more effective in reducing false positives. Both the CNN and XGBoost models achieved similar AUROC and Area Under the Precision-Recall Curve (AUPRC) of 0.99 (**Figure 9**). These metrics indicate promising sensitivity and precision.

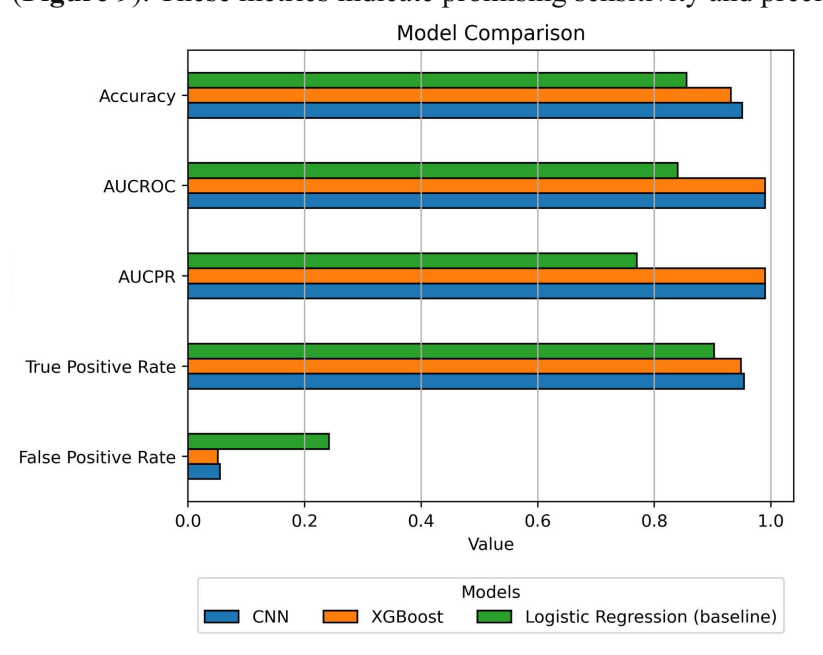


Figure 8: Comparative Analysis of Machine Learning Models. Horizontal bar chart illustrating the performance of three machine learning models: Convolutional Neural Network (CNN), XGBoost, and Logistic Regression (baseline). The metrics used for comparison are Accuracy, True Positive Rate, False Positive Rate, Area Under the Receiver Operating Characteristic Curve (AUCROC), and Area Under the Precision-Recall Curve (AUCPR). The CNN model exhibits the highest accuracy, while the Logistic Regression model serves as the baseline for comparison. Related statistics are listed in Table 4.

Metric	Comparison	Difference Estimate	95% CIs for differences	p-value	Significance
Accuracy	CNN vs. XGB	0.0196	(0.0107, 0.0285)	1.59x10 <sup>-5</sup>	***
	CNN vs. LR	0.0952	(0.0842, 0.1062)	1.21x10 <sup>-62</sup> (~0)	***
	XGB vs. LR	0.0756	(0.0640, 0.0872)	5.18x10 <sup>-37</sup> (~0)	***
AUCROC	CNN vs. XGB	0.0000	(-0.0038, 0.0038)	1.00	NS
Area Under the Receiver Operating	CNN vs. LR	0.1500	(0.1399, 0.1601)	2.21x10 <sup>-171</sup> (~0)	***
Characteristic Curve	XGB vs. LR	0.1500	(0.2452, 0.2748)	2.21x10 <sup>-171</sup> (~0)	***
AUCPR	CNN vs. XGB	0.0000	(-0.0038, 0.0038)	1.00	NS
(Area Under the Precision-	CNN vs. LR	0.2200	(0.2084, 0.2316)	2.71x10 <sup>-270</sup> (~0)	***
Recall Curve)	XGB vs. LR	0.2200	(0.2084, 0.2316)	2.71x10 <sup>-270</sup> (~0)	***
TPR	CNN vs. XGB	0.0051	(-0.0031, 0.0133)	0.22	NS

(True Positive Rate)	CNN vs. LR	0.0510	(0.0412, 0.0606)	$1.51 \times 10^{-24} (\sim 0)$	***
	XGB vs. LR	0.0458	(0.0359, 0.0557)	1.36x10 <sup>-19</sup> (~0)	***
FPR	CNN vs. XGB	0.0039	(-0.0046, 0.0124)	.367	NS
(False Positive Rate)	CNN vs. LR	-0.1870	(-0.2000, -0.1740)	5.20x10 <sup>-164</sup> (~0)	***
	XGB vs. LR	-0.1909	(-0.2038, -0.1780)	1.08x10 <sup>-172</sup> (~0)	***

Table 4: Comparative analysis of performance metrics between the Convolutional Neural Network (CNN), XGBoost (XGB), and Logistic Regression (LR) models (related to Figure 8). The CNN model shows comparable performance to the XGB model across all metrics, except accuracy for which it outperforms. Both CNN and XGB show significantly better performance than the LR model across most metrics. The p-values indicate the statistical significance of these differences, with smaller values indicating stronger evidence of a difference. Significance level notation after applying Bonferroni correction for multiple testing: 0.05 (\*), 0.01 (\*\*), 0.001(\*\*\*).

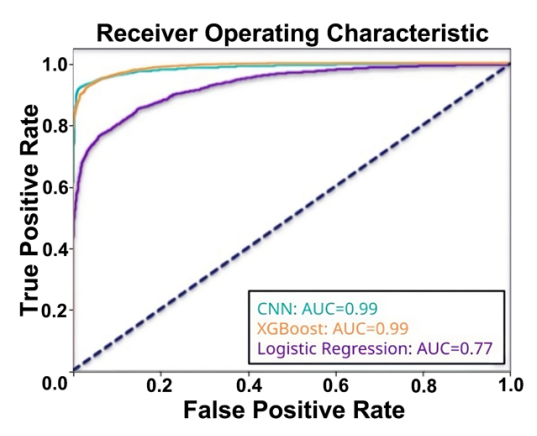


Figure 9: Receiver Operating Characteristic (ROC) Curves and Areas Under Curves (AUC) for Convolutional Neural Network (CNN), XGBoost, and Logistic Regression Classifiers. A ROC curve demonstrates the performance of an ABR classifier at all classification thresholds. The area under the ROC curve represents the ABR classifier's overall ability to distinguish between ABR responses that are above the hearing threshold and those that are not under varying model settings. The ROC curves for the CNN and XGBoost classifiers are nearly identical, while the Logistic Regression classifier shows relatively inferior performance.

In **Figure 10**, we compare the performance of three classifiers: Convolutional Neural Network (CNN), XGBoost, and Logistic Regression. We also include an Inter-Rater comparison, which reflects the proportion of ABRs for which two experts agree on a threshold within some envelope (within 5dB SPL, 10dB SPL, etc.), providing a real-world benchmark for performance.

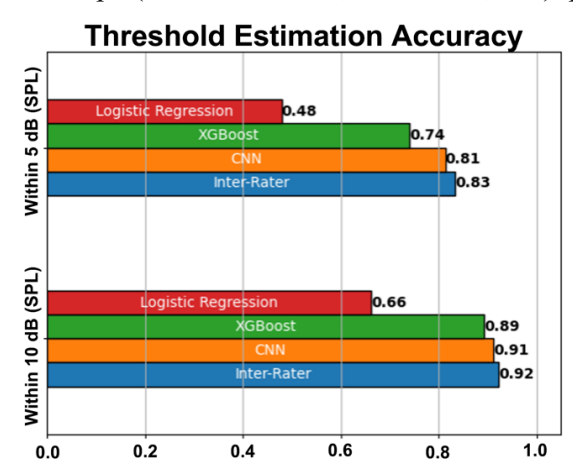


Figure 10: Threshold Estimation Metrics for Machine Learning Models and Human Expert Inter-Rater Comparison (statistics in Table 5). Bar chart comparing the performance of three machine learning models: Convolutional Neural Network (CNN), XGBoost, and Logistic Regression, as well as an Inter-Rater comparison based on their ability to estimate thresholds within 5dB SPL and 10dB SPL. The Inter-Rater comparison was conducted by comparing 100 threshold estimates of two experts. The CNN and XGBoost models demonstrate superior performance compared to the Logistic Regression model, with the CNN outperforming XGBoost at higher levels of precision. The Inter-Rater comparison provides a benchmark for human expert performance in the task.

The classifiers are evaluated based on their ability to estimate hearing thresholds, defined as the minimum sound intensity (in decibels) at a given frequency that elicits a repeatable neural response. The evaluation accuracy considers how frequently the estimated threshold falls within 5dBs or 10dBs of the single-rater ground truth threshold. **Table 5** provides inferential statistics for the differences between each model and inter-rater assessment at both accuracy envelopes. The CNN was the only model which performed comparably to human-rater assessment at the 10dB accuracy window; however no model could reach such accuracy at the 5dB envelope.

Accuracy Envelope	Comparison	Accuracy Difference	95% CIs for Accuracy Difference	p-value	Significance
Within 5dB SPL	CNN vs. IRR	0.02	(-0.0852, 0.1252)	0.7062	NS
	XGB vs. IRR	0.09	(-0.0154, 0.1955)	0.0545	NS
	LR vs. IRR	0.35	(0.2443, 0.4558)	7.992x10 <sup>-12</sup>	***
Within 10dB SPL	CNN vs. IRR	0.01	(-0.0673, 0.0874)	0.8628	NS
	XGB vs. IRR	0.03	(-0.0476, 0.1075)	0.4300	NS
	LR vs. IRR	0.26	(0.1814, 0.3387)	8.718x10 <sup>-8</sup>	***

Table 5: Inference for differences in accuracy between inter-rater accuracy and the Convolutional Neural Network (CNN), XGBoost (XGB), and Logistic Regression (LR) models (related to Figure 10). Within both the 5dB and 10dB envelopes, no significant difference between the CNN and XGB models and baseline inter-rater accuracy was detected, suggesting CNN and XGB are performing at a comparable level as a human reviewer; however LR did show significantly worse performance than inter-rater assessment. Significance level notation after applying Bonferroni correction for multiple testing: 0.05 (\*), 0.01 (\*\*), 0.001(\*\*\*).

The CNN demonstrates superior performance across both metrics compared with the Logistic Regression and XGBoost models. Furthermore, the temporal nature of the data is well-suited to the architecture of CNNs. Unlike traditional machine learning models, CNNs can effectively capture temporal dependencies in the data, which is crucial for tasks involving time-series data, such as our case of audio signal processing. The CNN model's superior performance at the 5dB and 10dB envelopes along with its ability to handle the temporal nature of the data makes it the optimal choice for this task. Moreover, the CNN achieves similar performance as the Inter-Rater comparison, indicating that its ability to estimate hearing thresholds is on par with the consensus of two human experts using standard visual threshold inspection methods. This suggests that the CNN model can function as a reliable tool for estimating hearing thresholds, providing a machine learning-based approach that matches human expert performance.

Metric \ Software	EPL-ABR	ABRA	
Accuracy	93.12 (±1.476)%	93.42 (±1.446)%	
True Positive Rate	97.10 (±0.978)%	90.00 (±1.749)%	
False Positive Rate	14.52 (±2.055)%	0.00 (±0.0)%	
Within 5dB SPL	57.14 (±2.886)%	91.42 (±1.633)%	
Within 10dB SPL	91.43 (±1.633)%	94.29 (±1.353)%	
Within 15dB SPL	94.29 (±1.353)%	94.29 (±1.353)%	

Table 6: Performance Comparison of Threshold Estimation Algorithms on Lab C data only (292 ABR waveforms from 27 mice). This table presents a side-by-side comparison of two threshold estimation algorithms: EPL-ABR and ABRA. The metrics used for comparison include Accuracy, True Positive Rate, False Positive Rate, and the ability to estimate thresholds within 5dB, 10dB, and 15dB. The values are presented as mean (± standard error). ABRA demonstrates superior performance (bolded) in terms of accuracy and estimating thresholds within 5dB, while EPL-ABR has a higher True Positive Rate.

The performance of our threshold estimation technique was compared against that of EPL-ABR (Suthakar & Liberman 2019) on a separate dataset of ABR waveforms from Lab C (**Table 6**). This smaller set of ABR waveforms (N = 292) was selected because EPL-ABR's threshold estimation software requires data in the custom ABR file format used by the Eaton Peabody Laboratories. Our CNN method outperforms EPL-ABR's threshold estimation method across all metrics except for FPR. One benefit of CNN is that it can be continuously trained and improved as more data is made available.

#### **Time Cost Analysis**

In order to quantify the time savings of using ABRA, we sent a random sample of 10 ABR files from Lab B to two ABR raters from Lab A with a total of 90 frequencies to be analyzed. It took both raters approximately 1 hour to manually analyze the ABR thresholds. However, using ABRA, it took about 48 seconds to output the automated thresholds for each frequency, corresponding to 75x increased efficiency. The automated thresholds were within 5 dBs of Lab A inspection 73% of the time, 10 dBs 88% of the time, and 15 dBs 96% of the time. For comparison, inter-rater assessment showed that a Lab A annotator was within 5 dB of a Lab B annotator's result 89% of the time, 10 dB 99% of the time, and 15 dB 100% of the time.

#### Discussion

The aim of this study is to illustrate ABRA's versatility and additional benefits compared to other available software such as ABRWAS and EPL-ABR (see **Table 7**). ABRA has been designed to be a multi-purpose and versatile software with extended functionality and to be able to handle input data acquired from different mouse strains, different laboratories, and recorded in different formats, including the widely used standard .arf files from BioSigRZ Tucker Davis

Technology recordings, or .csv files from any number of other systems given limited rules related to file structure.

FEATURES	ABRA	ABRWAS	EPL-ABR
Threshold Detection	Automated thresholding with both supervised/unsupervised machine learning methods	No automated threshold estimation	Automated thresholding using cross-covariance calculations
Peak Detection	Automates peak and trough detection	Suggests peak and trough detection as a guide for human revision	Automates peak and trough detection and allows for human revision
Time Warping	Performs elastic time warping	No time warping	No time warping
<b>Batch Processing</b>	Supports batch processing	Supports batch processing	No batch processing
Data Extraction	Generate peaks, troughs, and a metrics table with a single click	Generates peaks and troughs with option to manually adjust labels	Generates peaks and troughs with option to manually adjust labels
Metric Exports	Metrics table only includes three waveform metrics and the threshold for each frequency	Comprehensive metrics table	Comprehensive metrics table
Accessibility	Free and open source	Free and open source	Free and open source
Image Exports	Can export .png and .pdf files	No functionality	No functionality
Stability	When errors arise, app can recover easily	Errors require software relaunch	When errors arise, app can recover easily
File Type Support	Accepts .arfs and .csvs; only a couple rules related to the file structure	Each file must follow the same structure	Only supports EPL file type
Operating System	Windows/Mac/Linux	Windows	Windows/Mac
Web Support	Web-based application that can also run locally	Run on local machines only	Run on local machines only

**Table 7: Comparison of software features/capabilities.** Functionality and aspects of ABRA, the Auditory Brainstem Response Waveform Analyzer (ABRWAS) (Burke et al. 2023), and the EPL-ABR Peak Analysis App (Suthakar and Liberman 2019).

The tests done in the Manor lab have shown that ABRA's automated thresholding method reduces the time costs of thresholding analyses by more than 50x, and can help streamline the process of extracting ABR thresholds from multiple subjects. In addition, the results can be

exported to a .csv file for post-processing by the experimenter, and plots can be directly exported for publication if desired.

The deep learning techniques used in ABRA have some precedence not only in previous ABR studies but in the field of electrophysiology in general. A recent study showed that convolutional neural networks and long short-term memory architecture can automatically detect discrete records of protein movement (Celik et. al. 2020). Another electrophysiological study introduced a deep learning algorithm that infers latent dynamics from single-trial neural spiking data (Pandarinath et. al. 2018). This study used data from non-overlapping recording sessions that improved the inference of their model, similar to how our software accounts for a range of data collection protocols for improved generalizability. Both studies were designed to automate otherwise laborious and arduous tasks and simplify them such that future studies can be more accurate, more reproducible, and less time-consuming. The deep learning techniques used in our software have similar potential for ABR studies by streamlining the onerous task of labeling peaks and identifying thresholds. We envision future ABR acquisition protocols that can be guided by our software to avoid acquiring excess measurements after a threshold is reached.

While we have argued that ABRA is a powerful tool for ABR analysis, it is necessary to remark that it also has its limitations and there exist areas for future improvements. Currently ABRA can handle .csv and BioSigRZ .arf file inputs reliably, however functionality for analysis of BioSigRP .arf files is still in development. Calculation of amplitude/latency results and performing visualization when batch processing large numbers of ABR files (N>100 waveforms) may take several minutes, especially if the user chooses to implement the time warping functionality. ABRA developers are currently investigating the feasibility of moving computation to cloud-hosted GPUs to accelerate data processing. Similarly, quality of life improvements for manual relabeling of ABRA-generated peaks, latencies, and thresholds are also an area for future work. As for model limitations, the CNN-based thresholding model was trained only on mouse ABRs which had step sizes no larger than 20 dB SPL. Moreover, it was validated for automated amplitude and latency measurements for only Wave 1, leaving the remaining Waves 2-5 currently unvalidated, which can be pursued in future efforts as the model continues to incorporate new data from our labs and others. Most importantly, the accuracy of peak and threshold detection may not yet match that of the most seasoned experts in visual ABR analysis. While the time saved by automation may still yet be a worthwhile tradeoff for certain applications, an additional benefit is the deterministic nature of the model and therefore high reproducibility. Most importantly, we anticipate significant improvements in performance as the amount of training data is increased over time.

Overall, this study has shown that the ABRA interface is a flexible one-stop-shop software for ABR amplitude/latency estimation, thresholding, visualization, and all plots can be exported for

generating figures. ABRA's ease-of-use, generalizability, and diverse functionality serve as potential outlets to streamline data processing and resulting studies involving ABR analysis.

#### Acknowledgements

We would like to thank Kirupa Suthakar and Charles Liberman for providing us with data as well as helping us improve our software, Zhijun Shen and Mark Rutherford, and Kali Burke and Amanda Lauer for helping us improve our software and for their insightful feedback on the manuscript. U.M. is supported by a CZI Imaging Scientist Award (DOI:10.37921/694870itnyzk) from the Chan Zuckerberg Initiative DAF), NSF NeuroNex Award 2014862, the David F. And Margaret T. Grohne Family Foundation, the G. Harold & Leila Y. Mathers Foundation, NIDCD R018566-03S1 and R01 DC021075-01, and the UCSD Goeddel Family Technology Sandbox. The collection of Marcotti Lab data was supported by an Innovation Seed Fund from the RNID (F115) to F.C. and BBSRC grant (BB/V006681/1) to W.M.

#### References

Bao, Jianxin, Segun Light Jegede, John W. Hawks, Bethany Dade, Qiang Guan, Samantha Middaugh, Ziyu Qiu, Anna Levina, and Tsung-Heng Tsai. "Detecting Cochlear Synaptopathy through Curvature Quantification of the Auditory Brainstem Response." *Frontiers in Cellular Neuroscience* 16 (2022). https://doi.org/10.3389/fncel.2022.851500.

Buran, Brad. "Auditory Wave Analysis". Zenodo, 2015. https://doi.org/10.5281/zenodo.17365.

Buran, Brad N., Garnett P. McMillan, Sarineh Keshishzadeh, Sarah Verhulst, and Naomi F. Bramhall. "Predicting synapse counts in living humans by combining computational models with auditory physiology." *The Journal of the Acoustical Society of America* 151, no. 1 (2022): 561-576.

Burkard, Robert, and Manny Don. "The auditory brainstem response (ABR)." *Translational Perspectives in Auditory Neuroscience: Hearing Across the Life Span—Assessment and Disorders. San Diego, CA: Plural Publishing* (2012): 161-200.

Bramhall, Naomi F., Garnett P. McMillan, Sharon G. Kujawa, and Dawn Konrad-Martin. "Use of non-invasive measures to predict cochlear synapse counts." *Hearing research* 370 (2018): 113-119.

Burke, Kali, Matthew Burke, and Amanda M. Lauer. "Auditory brainstem response (ABR) waveform analysis program." *MethodsX* 11 (2023): 102414. https://doi.org/10.1016/j.mex.2023.102414.

Celik, Numan, Fiona O'Brien, Sean Brennan, Richard D. Rainbow, Caroline Dart, Yalin Zheng, Frans Coenen, and Richard Barrett-Jolley. "Deep-Channel uses deep neural networks to detect single-molecule events from patch-clamp data." *Communications Biology* 3, no. 1 (2020): 3.

Eggermont, Jos J. "Auditory brainstem response." *Handbook of clinical neurology* 160 (2019): 451-464.

Fernandez, Katharine A., Penelope WC Jeffers, Kumud Lall, M. Charles Liberman, and Sharon G. Kujawa. "Aging after noise exposure: acceleration of cochlear synaptopathy in 'recovered' ears." *Journal of Neuroscience* 35, no. 19 (2015): 7509-7520. https://doi.org/10.1523/jneurosci.5138-14.2015.

Henry, Kenneth R. "Auditory brainstem volume-conducted responses: origins in the laboratory mouse." *Ear and Hearing* 4, no. 5 (1979): 173-178.

Ingham, Neil J., Selina Pearson, and Karen P. Steel. "Using the auditory brainstem response (ABR) to determine sensitivity of hearing in mutant mice." *Current Protocols in Mouse Biology* 1, no. 2 (2011): 279-287.

Kamerer, Aryn M., Stephen T. Neely, and Daniel M. Rasetshwane. "A model of auditory brainstem response wave I morphology." *The Journal of the Acoustical Society of America* 147, no. 1 (2020): 25-31.

Kim, Ye-Hyun, Katrina M. Schrode, and Amanda M. Lauer. "Auditory brainstem response (ABR) measurements in small mammals." *Developmental, physiological, and functional neurobiology of the inner ear* (2022): 357-375.

Kleffe, Jürgen. "Principal components of random variables with values in a seperable hilbert space." *Mathematische Operationsforschung und Statistik* 4, no. 5 (1973): 391-406.

Land, Rüdiger, Alice Burghard, and Andrej Kral. "The contribution of inferior colliculus activity to the auditory brainstem response (ABR) in mice." *Hearing research* 341 (2016): 109-118.

McKearney, Richard M., and Robert C. MacKinnon. "Objective auditory brainstem response classification using machine learning." *International journal of audiology* 58, no. 4 (2019): 224-230.

McKearney, Richard M., Steven L. Bell, Michael A. Chesnaye, and David M. Simpson. "Auditory brainstem response detection using machine learning: a comparison with statistical detection methods." *Ear and Hearing* 43, no. 3 (2022): 949-960.

Melcher, Jennifer R., Inge M. Knudson, Barbara C. Fullerton, John J. Guinan Jr, Barbara E. Norris, and Nelson YS Kiang. "Generators of the brainstem auditory evoked potential in cat. I. An experimental approach to their identification." *Hearing research* 93, no. 1-2 (1996): 1-27.

Møller, A. R., & Jannetta, P. J. (1985). Neural generators of the auditory brainstem response. The auditory brainstem response, 13-31.

Pandarinath, Chethan, Daniel J. O'Shea, Jasmine Collins, Rafal Jozefowicz, Sergey D. Stavisky, Jonathan C. Kao, Eric M. Trautmann et al. "Inferring single-trial neural population dynamics using sequential auto-encoders." *Nature methods* 15, no. 10 (2018): 805-815.

Radziwon, Kelly E., Kristie M. June, Daniel J. Stolzberg, Matthew A. Xu-Friedman, Richard J. Salvi, and Micheal L. Dent. "Behaviorally measured audiograms and gap detection thresholds in CBA/CaJ mice." *Journal of Comparative Physiology A* 195 (2009): 961-969.

Rüttiger, Lukas, Ulrike Zimmermann, and Marlies Knipper. "Biomarkers for hearing

dysfunction: facts and outlook." Orl 79, no. 1-2 (2017): 93-111.

Schrode, Katrina M., Micheal L. Dent, and Amanda M. Lauer. "Sources of variability in auditory brainstem response thresholds in a mouse model of noise-induced hearing loss." *The Journal of the Acoustical Society of America* 152, no. 6 (2022): 3576-3582.

Simpson, M. I., and Garreth Prendergast. 2013. "Auditory Magnetic Evoked Responses." In *Handbook of Clinical Neurophysiology*, 10:253–70. Elsevier.

"Streamlit, a Faster Way to Build and Share Data Apps," n.d. https://streamlit.io/.

Suthakar, Kirupa, and M. Charles Liberman. "A simple algorithm for objective threshold determination of auditory brainstem responses." *Hearing research* 381 (2019): 107782.

Takeda, Toshio, Masanori Hosokawa, Shuji Takeshita, Mika Irino, Keiichi Higuchi, Takatoshi Matsushita, Yumiko Tomita et al. "A new murine model of accelerated senescence." *Mechanisms of ageing and development* 17, no. 2 (1981): 183-194.

Tucker, J. D. "fdasrsf: Functional data analysis using the square root slope framework." *GitHub Repository. GitHub, https://github. com/jdtuck/fdasrsf python* (2021).

Wimalarathna, Hasitha, Sangamanatha Ankmnal-Veeranna, Chris Allan, Sumit K. Agrawal, Prudence Allen, Jagath Samarabandu, and Hanif M. Ladak. "Comparison of machine learning models to classify auditory brainstem responses recorded from children with auditory processing disorder." *Computer methods and programs in biomedicine* 200 (2021): 105942.

Xie, Lihong, Menglin Wang, Ting Liao, Songhua Tan, Kai Sun, Heng Li, Qin Fang, and Anzhou Tang. "The characterization of auditory brainstem response (ABR) waveforms: A study in tree shrews (Tupaia belangeri)." *Journal of otology* 13, no. 3 (2018): 85-91.

Young, Allen, Jennifer Cornejo, and Alycia Spinner. "Auditory brainstem response." In *StatPearls [Internet]*. StatPearls Publishing, 2023.

SGNs CN CN SOC LL

AN SOC LL

SOC LL

LC

LC

A

IC

LC

A

IC

A

IC

Time (ms)

ABR waveform recorded from a mouse showing its characteristic feature, wave 2 by the cochlear nucleus (CN), Wave 3 by the superior olivary cove 5 by the inferior colliculus (IC) (Rittiger et. al. 2017). Peaks of these waves a specific part of these waves a specific part of these waves a specific part of the second part of the se

**ABR Waves 1-5 (Mouse)** 

the auditory nerve (AN), Wave 2 by the cochlear nucleus (CN), Wave 3 by the superior olivary complex (SOC), Wave 4 by lateral Figure 1: Example of ABR waveform recorded from a mouse showing its characteristic features or waves. Wave 1 is generated by lemniscus (LL), and Wave 5 by the inferior colliculus (IC) (Rüttiger et. al. 2017). Peaks of these waves are denoted by red dots, and

troughs with blue dots.

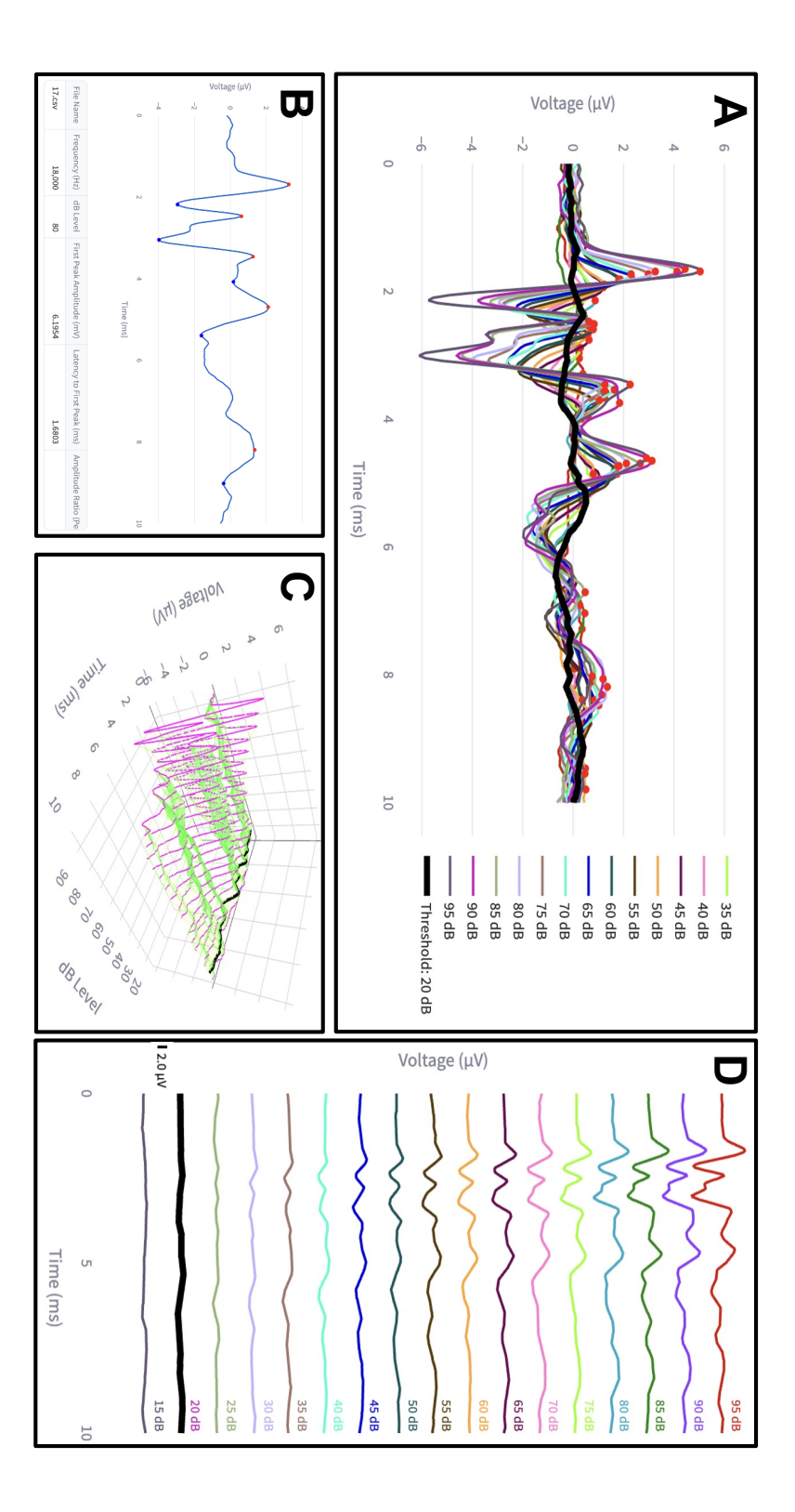
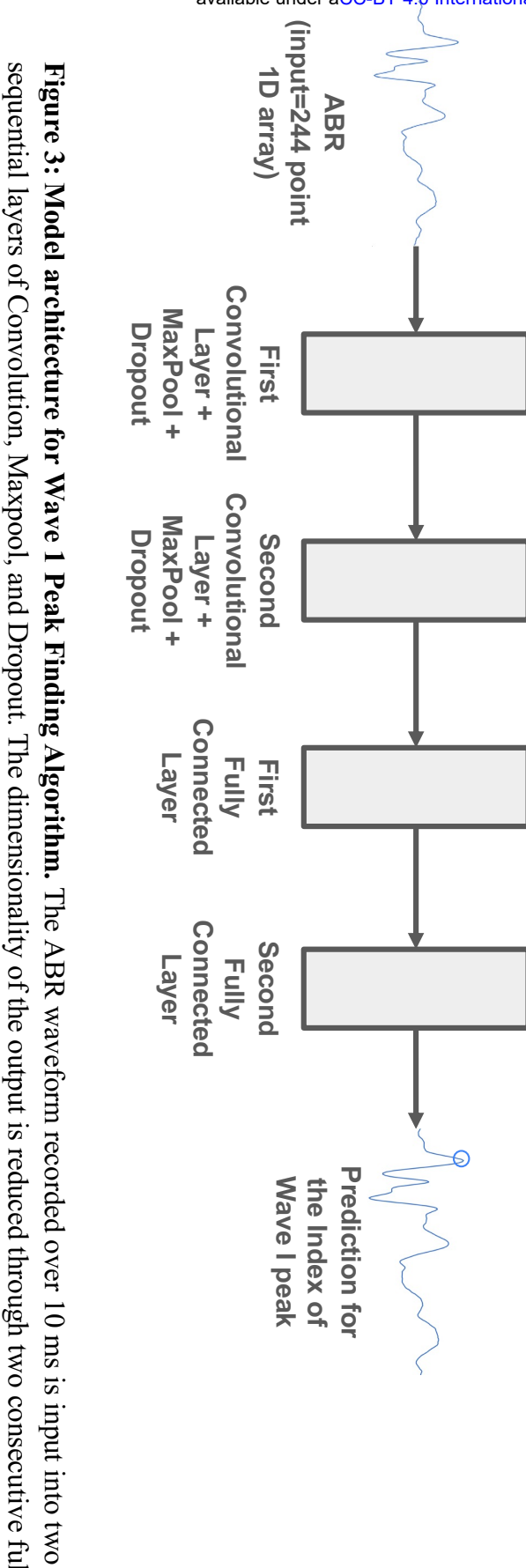
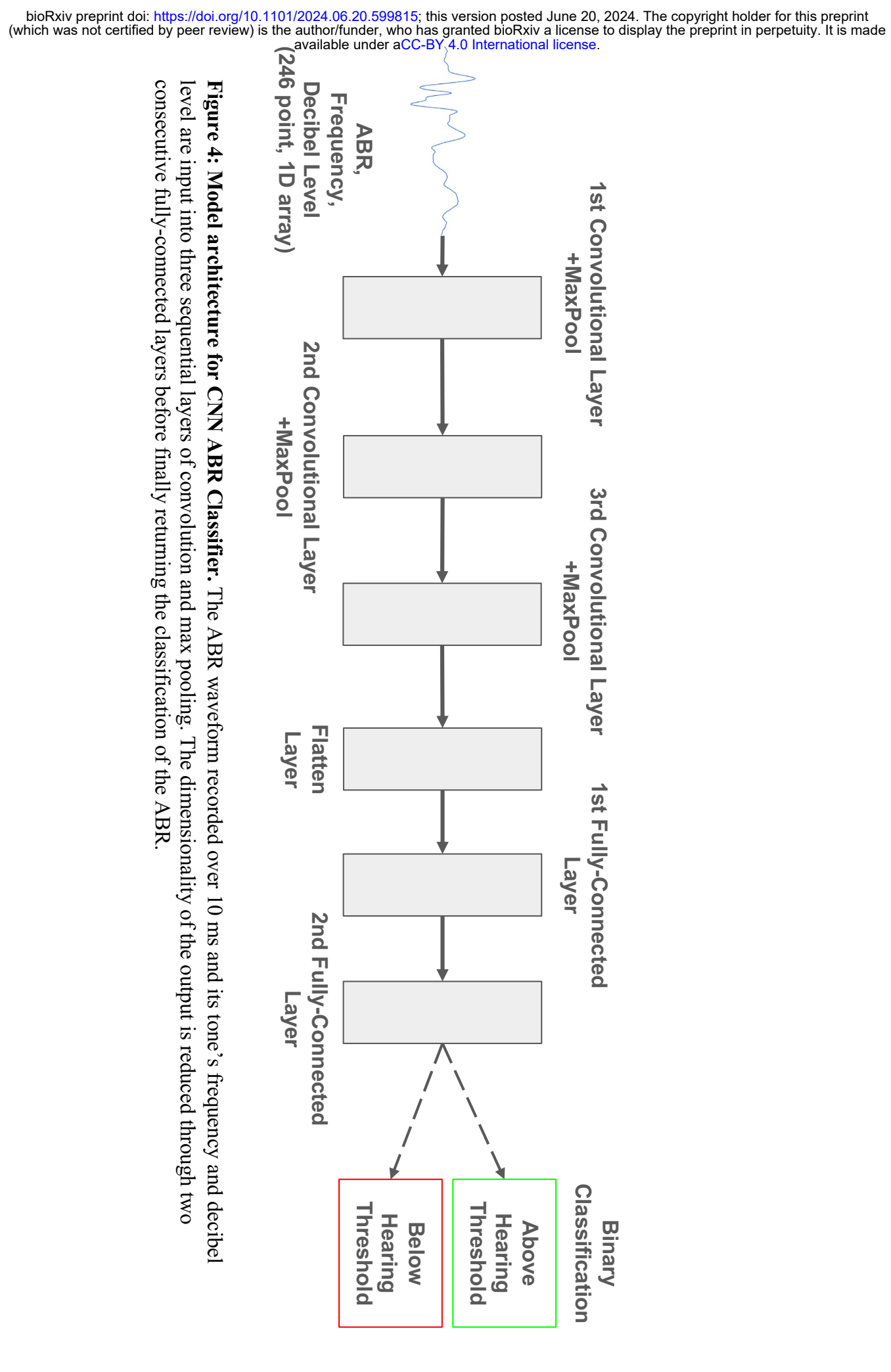


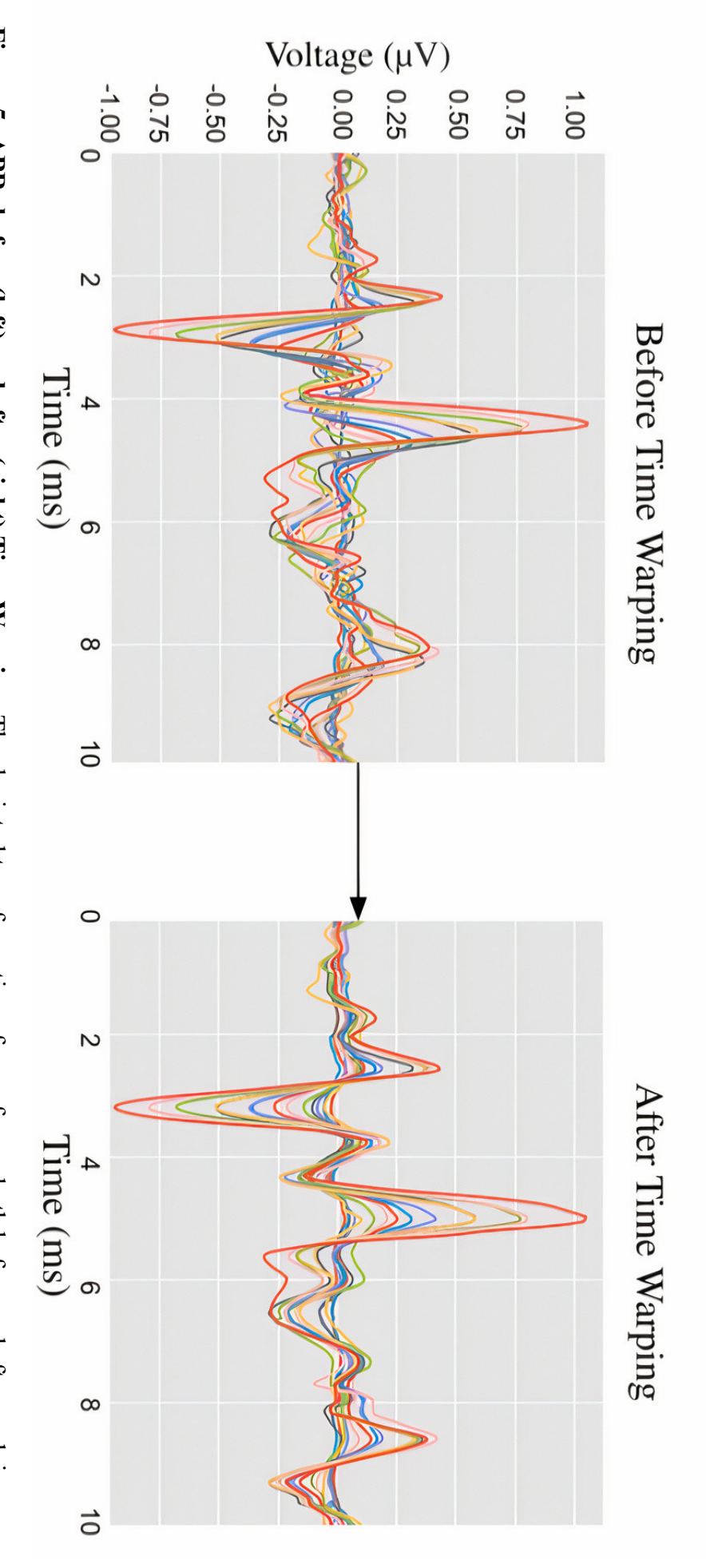
Figure 2: Screenshots from the ABRA app highlighting the different functionalities of ABRA (A) visualizing several ABR predicted threshold (20dB) highlighted in black. in black (can be rotated in the app) (D) stacks of ABR waveforms as a function of increasing dB SPL from the same frequency with the peaks and troughs labeled. ( $\mathbf{C}$ ) 3D plotting of all ABR waveforms at a given frequency with the predicted threshold (20dB) highlighted predicted threshold (thick black line). (B) plotting a single ABR waveform at a specific sound frequency and intensity (dB SPL) with waveforms from one 1 mo male C57Bl/6N mouse across different togglable dBs at 18kHz with predicted peak locations (red points) and



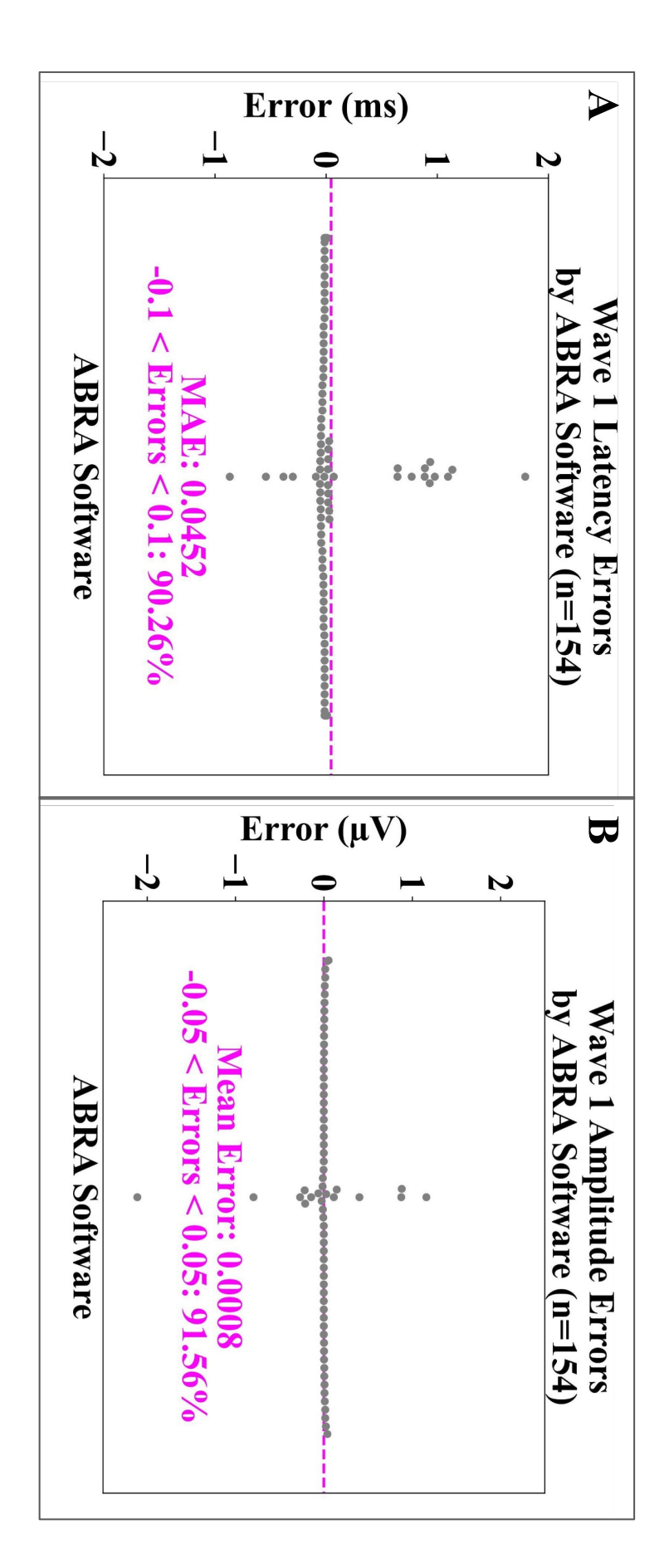
connected layers which returns the prediction of the time point of the Wave 1 peak. sequential layers of Convolution, Maxpool, and Dropout. The dimensionality of the output is reduced through two consecutive fully-



consecutive fully-connected layers before finally returning the classification of the ABR. level are input into three sequential layers of convolution and max pooling. The dimensionality of the output is reduced through two Figure 4: Model architecture for CNN ABR Classifier. The ABR waveform recorded over 10 ms and its tone's frequency and decibel



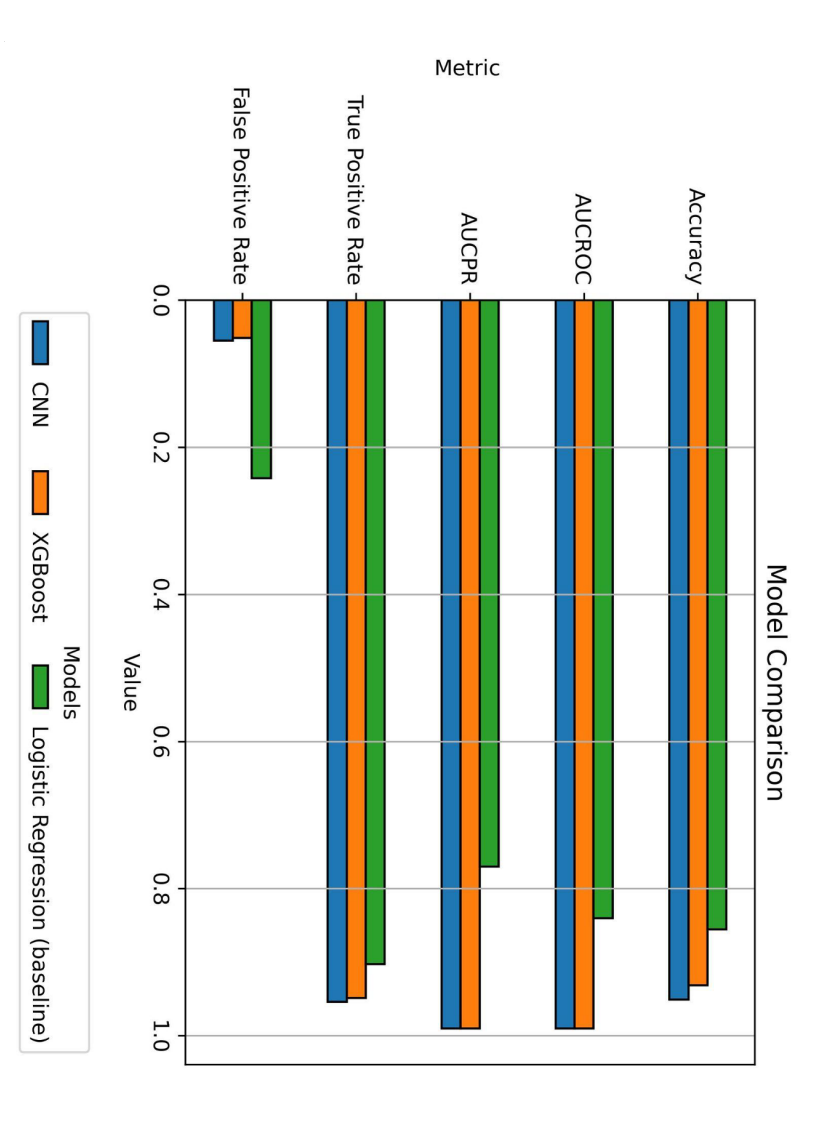
aligned latencies for all wave peaks and troughs. elastic time warping using the fdasrsf package (Tucker 2020), illustrates clear registration of waveform features. Associated with each waveform is also an estimated time warping function which is useful in quantifying changes between the original unaligned latencies to the Figure 5: ABRs before (left) and after (right) Time Warping. The depicted transformation of waveforms, both before and after applying



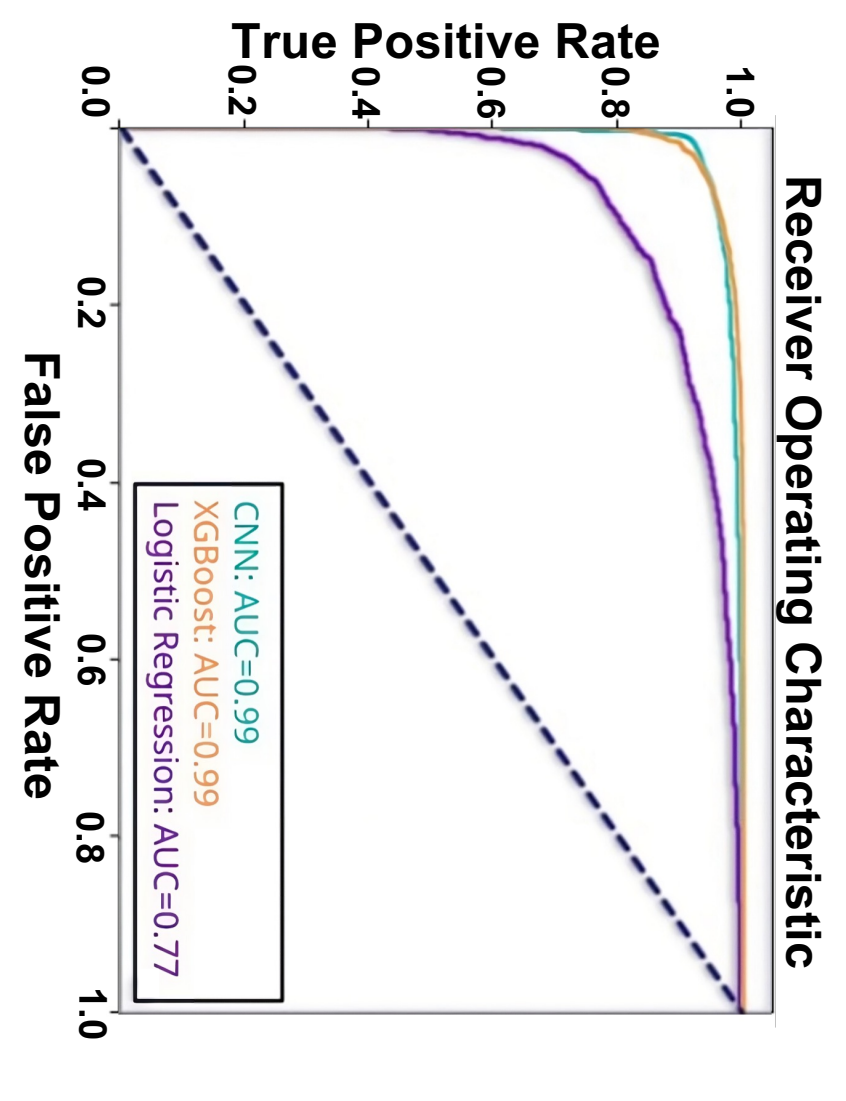
corresponding true human-labeled latency; 91.56% of all ABRA-generated Wave 1 amplitude were within 0.05 μV of the corresponding true human-labeled peak amplitude each software. Testing failed to find evidence that mean absolute errors were significantly greater than zero for both Wave 1 Figure 6: Swarmplots displaying spreads of error for detected Wave 1 Latency (A) and Amplitude (B) vs. ground truth for Latency and Amplitude estimates. 90.26% of all ABRA-generated estimates of Wave 1 Latency were within 0.1ms of the

Voltage (μV) Voltage (μV) -1.5 -1.0-0.50.0 0.5 -1.51.0 1.5 -0.50.0 0.5 1.0 1.5 Frequency (kHz)=18, Decibel (dB SPL)=90 Frequency (kHz)=16, Decibel (dB SPL)=90 ABRA Detected Latency Ground Truth 4 6 Time (ms) Time (ms) 10 10 Voltage (µV) Voltage (µV) B -1.5 -0.5-1.0 0.0 0.51.5 -1.5 -0.51.0 0.5 1.5 0.01.0 Frequency (kHz)=8, Decibel (dB SPL)=90 Frequency (kHz)=4, Decibel (dB SPL)=90 4 6 Time (ms) Time (ms) 10 10

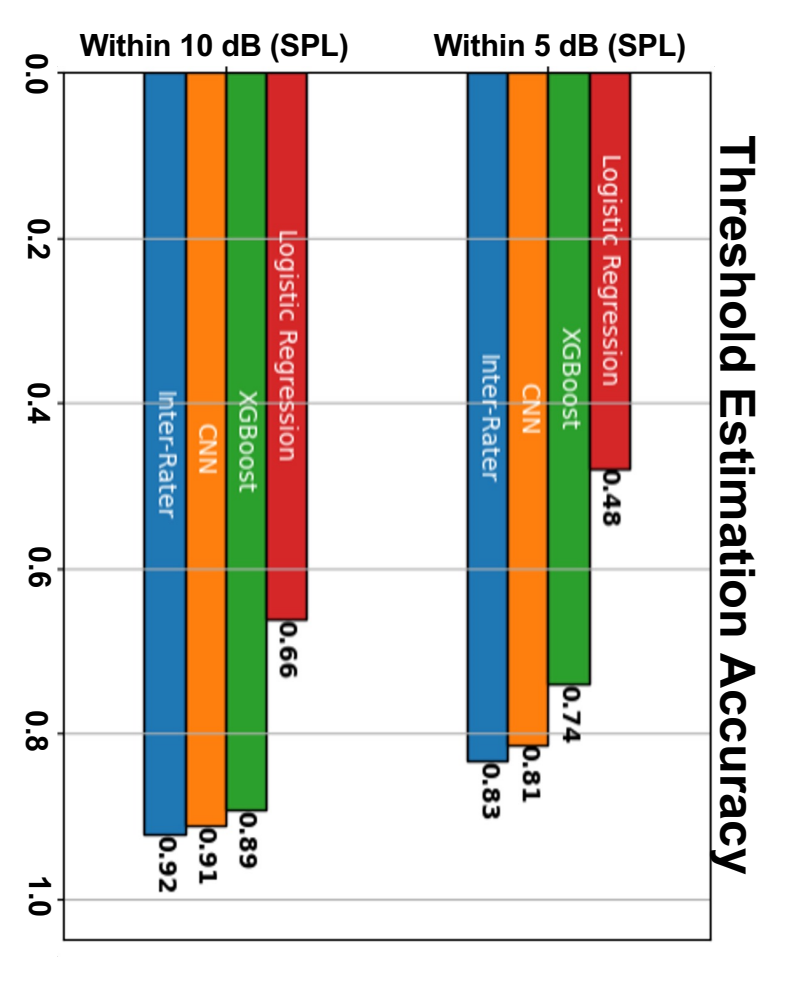
softwares and different sets of eyes. (B) ABRA may identify the incorrect peak. (C) and (D) are examples of ABR waveforms with larger signal to noise ratios for which ABRA matches the ground truth. Figure 7: Examples of error cases in peak detection. (A) example of multiple peaks that may be identified as Wave 1 by different



as the baseline for comparison are Accuracy, True Positive Rate, False Positive Rate, Area Under the Receiver Operating Characteristic Curve (AUCROC), and Area Under the Precision-Recall Curve (AUCPR). The CNN model exhibits the highest accuracy, while the Logistic Regression model serves Figure 8: Comparative Analysis of Machine Learning Models. Horizontal bar chart illustrating the performance of three machine learning models: Convolutional Neural Network (CNN), XGBoost, and Logistic Regression (baseline). The metrics used for comparison



at all classification thresholds. The area under the ROC curve represents the ABR classifier's overall ability to distinguish between Network (CNN), XGBoost, and Logistic Regression Classifiers. A ROC curve demonstrates the performance of an ABR classifier Figure 9: Receiver Operating Characteristic (ROC) Curves and Areas Under Curves (AUC) for Convolutional Neural performance ABR responses that are above the hearing threshold and those that are not under varying model settings. The ROC curves for the CNN and XGBoost classifiers are nearly identical, while that of the Logistic Regression classifier suggests relatively inferior



superior performance compared to the Logistic Regression model, with the CNN outperforming XGBoost at higher levels of precision comparison was conducted by comparing 100 threshold estimates of two experts. The CNN and XGBoost models demonstrate comparing the performance of three machine learning models: Convolutional Neural Network (CNN), XGBoost, and Logistic The Inter-Rater comparison provides a benchmark for human expert performance in the task. Regression, as well as an Inter-Rater comparison based on their ability to estimate thresholds within 5dB and 10dB. The Inter-Rater Figure 10: Threshold Estimation Metrics for Machine Learning Models and Human Expert Inter-Rater Comparison. Bar chart

# **Supplementary Information**

# Data Collection Methods

Detailed description of data collection methodology is described for each of the three labs as follows:

#### Manor Lab Data (Lab A)

- Anesthesia: 3 month SAMP8 (Senescence-Accelerated Mouse-Prone 8) (Takeda et al. 1981) mice were anesthetized using an intraperitoneal injection of a mixture of ketamine (90 mg/kg) and xylazine (10 mg/kg). If required to maintain anesthesia, mice received an additional quarter of the original dose as a top-up.
- Preparation: Ophthalmic ointment (Dechra) was applied to the subjects' eyes once anesthetized. Animals were placed in a soundproof chamber (IAC Acoustics, IL) to isolate them from exterior noise completely and a heating pad (Braintree Scientific Inc.) was used to maintain the temperature at 37°C.
- Electrode Placement: A recording electrode was inserted subcutaneously at the vertex and a reference electrode was placed behind the right pinna, with the ground electrode placed in the left leg.
- Sound Stimuli: Sound stimuli were presented via an MF1 Multi-field magnetic speaker (Tucker-Davis Technologies, TDT, FL) situated 10 cm from the mouse's right ear. Output stimuli were calibrated with a one-quarter-inch microphone (model PCB-378C01; PCB Piezotronics, NY) placed at the same distance from the speaker as the mouse ears would be.
- Recording: Electrophysiological signals in response to each tone stimulus were recorded for 10 ms starting at the onset of the tone. Stimuli were 5-ms tone pips (0.5 ms cos2 risefall) delivered at 21s with alternating stimulus polarity. Recorded electrical responses were filtered (300 Hz to 3 kHz) and averaged using BioSigRZ software (TDT, FL).
- Sound Intensity: The sound intensity level was decreased in 5 dB increments from 90 dB SPL to 10 or 20 dB SPL. At each sound level, 512 responses were averaged.

# Marcotti Lab Data (Lab B)

- Anesthesia: Female C57BL/6N mice were anesthetized using intraperitoneal injection of ketamine (100 mg/Kg body weight, Fort Dodge Animal Health, Fort Dodge, USA) and xylazine (10 mg/Kg, Rompun 2%, Bayer HealthCare LLC, NY, USA).
- Preparation: Following the onset of anesthesia and the loss of the retraction reflex with a toe pinch, mice were placed onto a heat mat (37°C) in a soundproof chamber (MAC-3 acoustic chamber, IAC Acoustic, UK).

- Electrode Placement: Subdermal electrodes were placed under the skin behind the pinna of each ear (reference and ground electrode) and on the vertex of the mouse (active electrode) as previously described (Ingham et al., 2011).
- Sound Stimuli: Sound stimuli were delivered to the ear by calibrated loudspeakers (MF1-S, Multi-Field Speaker, Tucker-Davis Technologies, USA) placed 10 cm from the animal's pinna. Sound pressure was calibrated with a low-noise microphone probe system (ER10B+, Etymotic, USA).
- Recording: Experiments were performed using a customized software (Ingham et al., 2011) driving an RZ6 auditory processor (Tucker-Davis Technologies). Auditory thresholds were estimated from the resulting ABR waveform and defined as the lowest sound level (measured in decibels, dB) where any recognizable feature of the waveform was visible.
- Sound Intensity: Stimulus sound pressure levels were typically 0-95 dB SPL, presented in steps of 5 dB SPL. The ABR response signal was averaged over 256 repetitions.

# Liberman Lab Data (Lab C)

- Anesthesia: 7 week C57Bl/6J mice were anesthetized using ketamine/xylazine anesthesia (Ketamine: 100 mg/kg, Xylazine: 10 mg/kg).
- Preparation: subjects were placed in a closed acoustic system.
- Electrode Placement: The response was recorded via needle electrodes inserted through the skin (vertex to ipsilateral pinna near tragus with a ground on the back near the tail).
- Sound Stimuli: Stimuli were 5-ms pips (0.5-ms rise-fall with a cos2 onset envelope, delivered at 30/sec).
- Recording: The response was amplified (10,000 X), filtered (100 Hz 3 kHz), and averaged with an A-D board in a LabVIEW-driven data-acquisition system.
- Sound Intensity: The sound level was raised in 5 dB steps from roughly 10 dB below the threshold up to 80 dB SPL. At each sound level, 1024 responses were averaged (with stimulus polarity alternated.

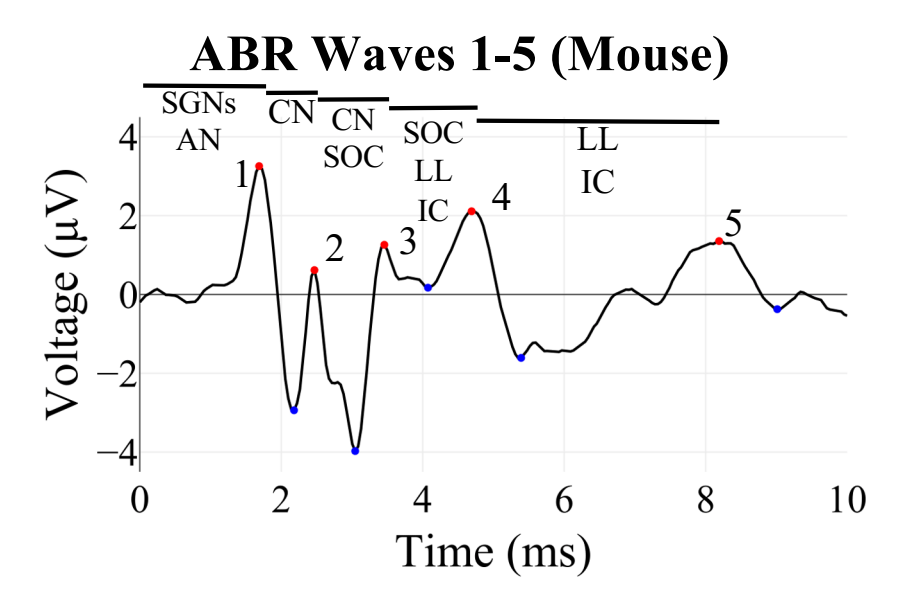


**Figure 1: Example of ABR waveform recorded from a mouse showing its characteristic features or waves.** Wave 1 is generated by the auditory nerve (AN), Wave 2 by the cochlear nucleus (CN), Wave 3 by the superior olivary complex (SOC), Wave 4 by lateral lemniscus (LL), and Wave 5 by the inferior colliculus (IC) (Rüttiger et. al. 2017). Peaks of these waves are denoted by red dots, and troughs with blue dots.

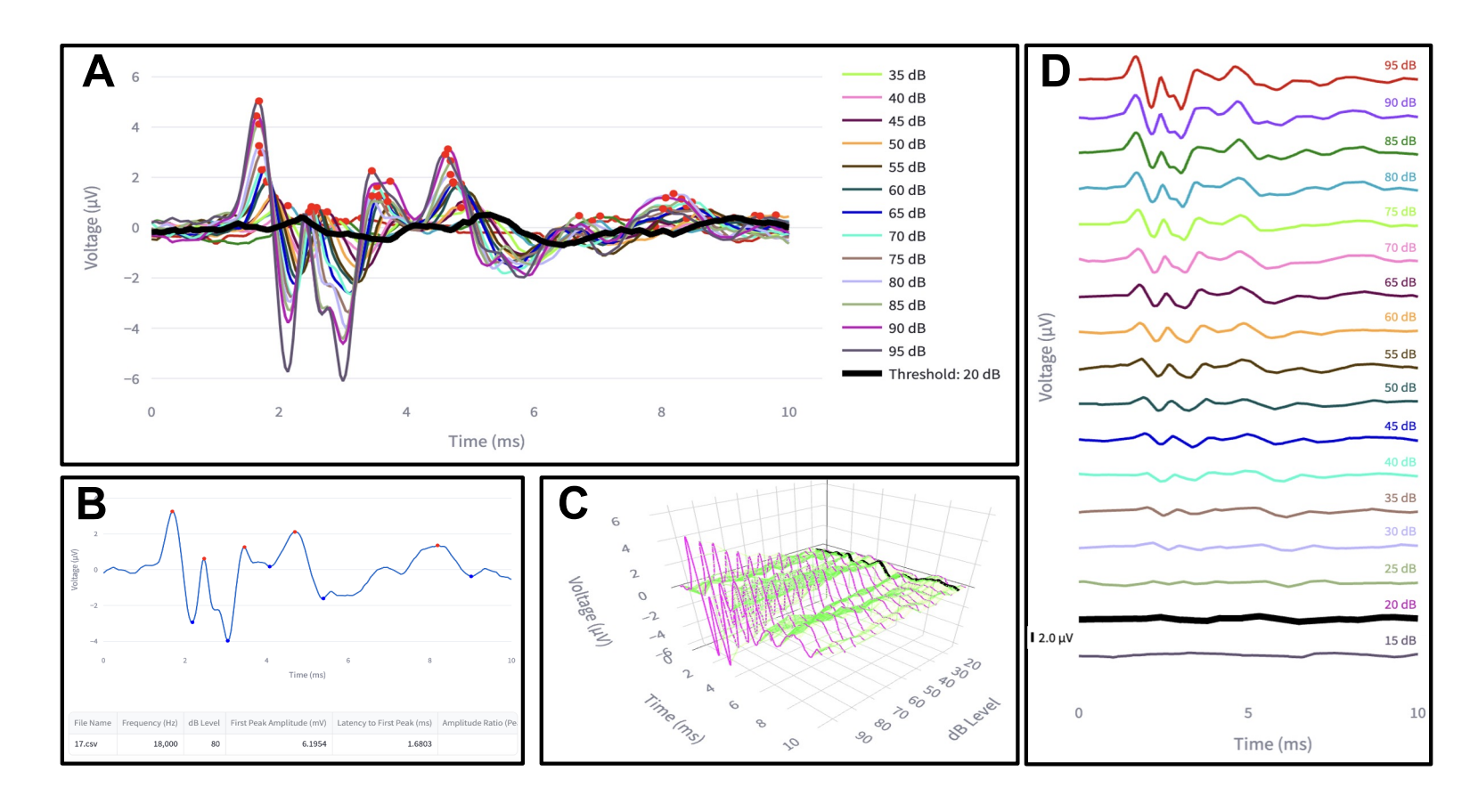
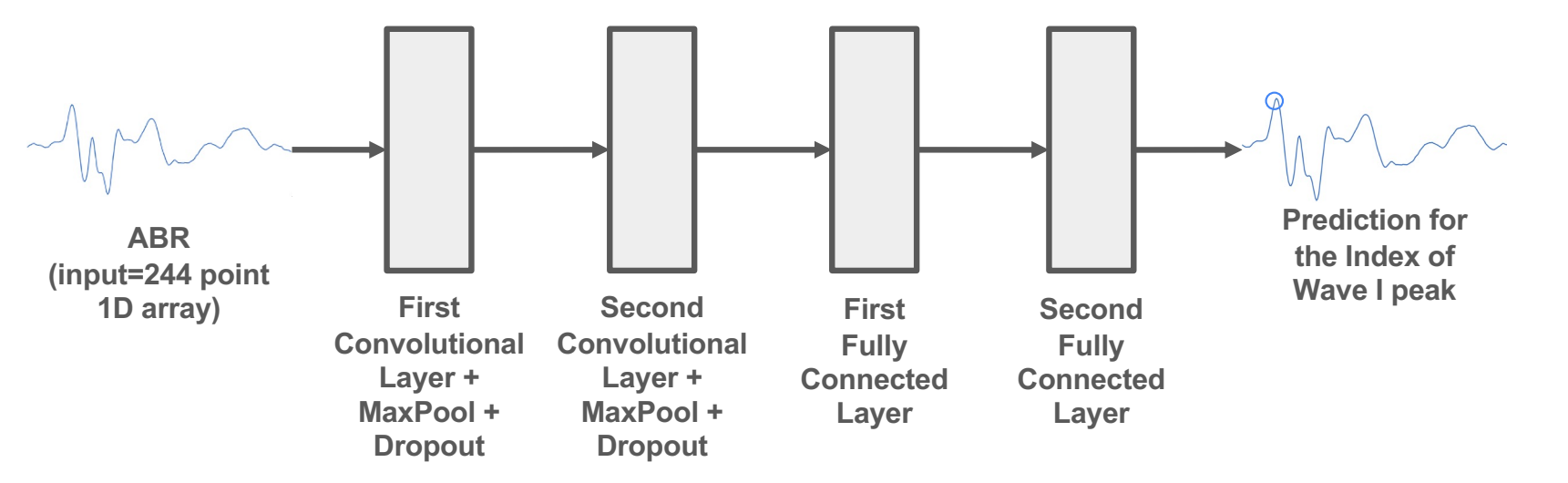
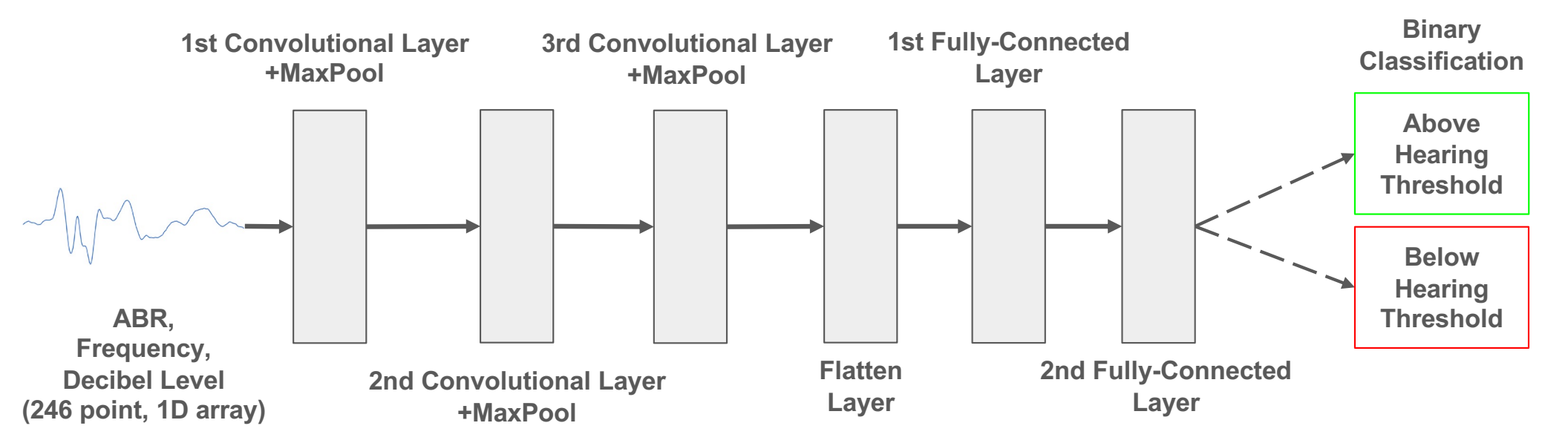


Figure 2: Screenshots from the ABRA app highlighting the different functionalities of ABRA (A) visualizing several ABR waveforms from one 1 mo male C57Bl/6N mouse across different togglable dBs at 18kHz with predicted peak locations (red points) and predicted threshold (thick black line). (B) plotting a single ABR waveform at a specific sound frequency and intensity (dB SPL) with peaks and troughs labeled. (C) 3D plotting of all ABR waveforms at a given frequency with the predicted threshold (20dB) highlighted in black (can be rotated in the app) (D) stacks of ABR waveforms as a function of increasing dB SPL from the same frequency with the predicted threshold (20dB) highlighted in black.



**Figure 3: Model architecture for Wave 1 Peak Finding Algorithm.** The ABR waveform recorded over 10 ms is input into two sequential layers of Convolution, Maxpool, and Dropout. The dimensionality of the output is reduced through two consecutive fully-connected layers which returns the prediction of the time point of the Wave 1 peak.



**Figure 4: Model architecture for CNN ABR Classifier.** The ABR waveform recorded over 10 ms and its tone's frequency and decibel level are input into three sequential layers of convolution and max pooling. The dimensionality of the output is reduced through two consecutive fully-connected layers before finally returning the classification of the ABR.

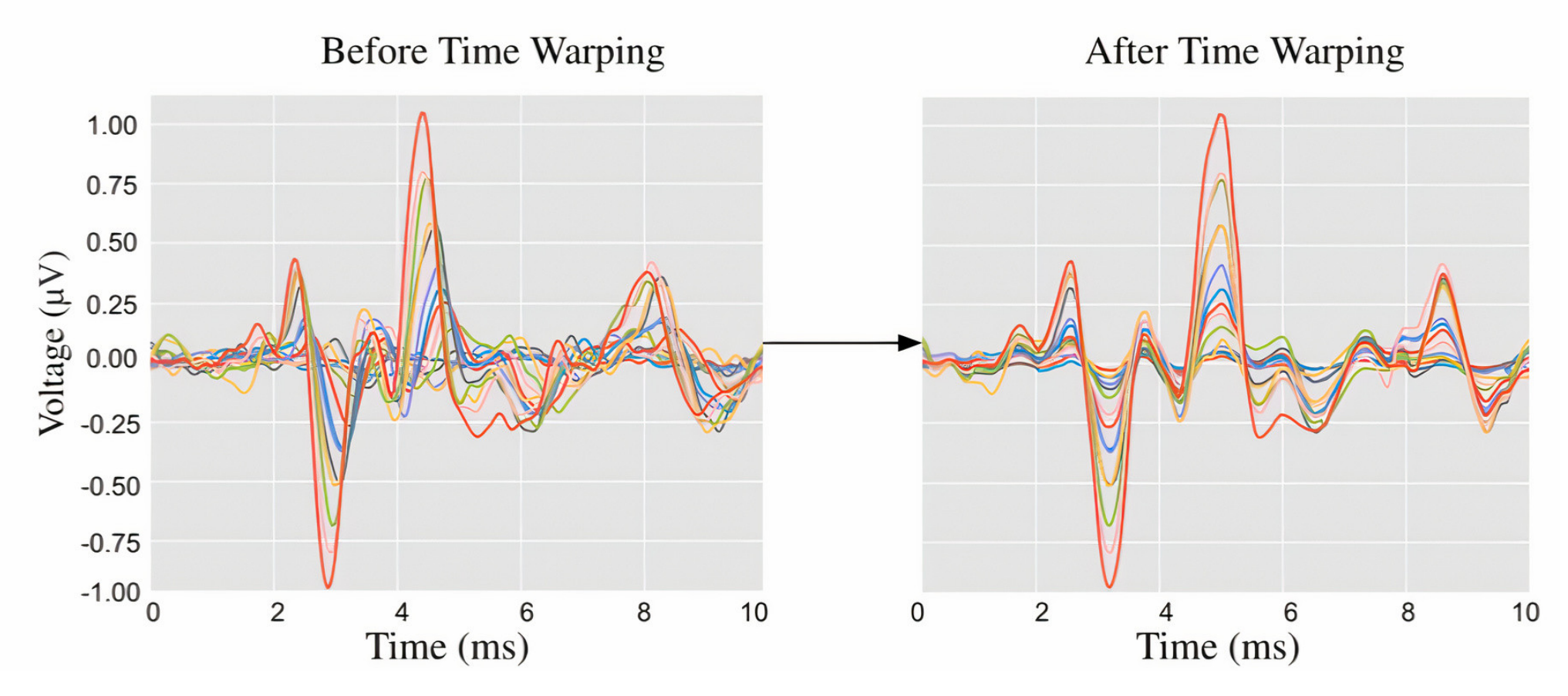


**Figure 5: ABRs before (left) and after (right) Time Warping.** The depicted transformation of waveforms, both before and after applying elastic time warping using the *fdasrsf* package (Tucker 2020), illustrates clear registration of waveform features. Associated with each waveform is also an estimated time warping function which is useful in quantifying changes between the original unaligned latencies to the aligned latencies for all wave peaks and troughs.

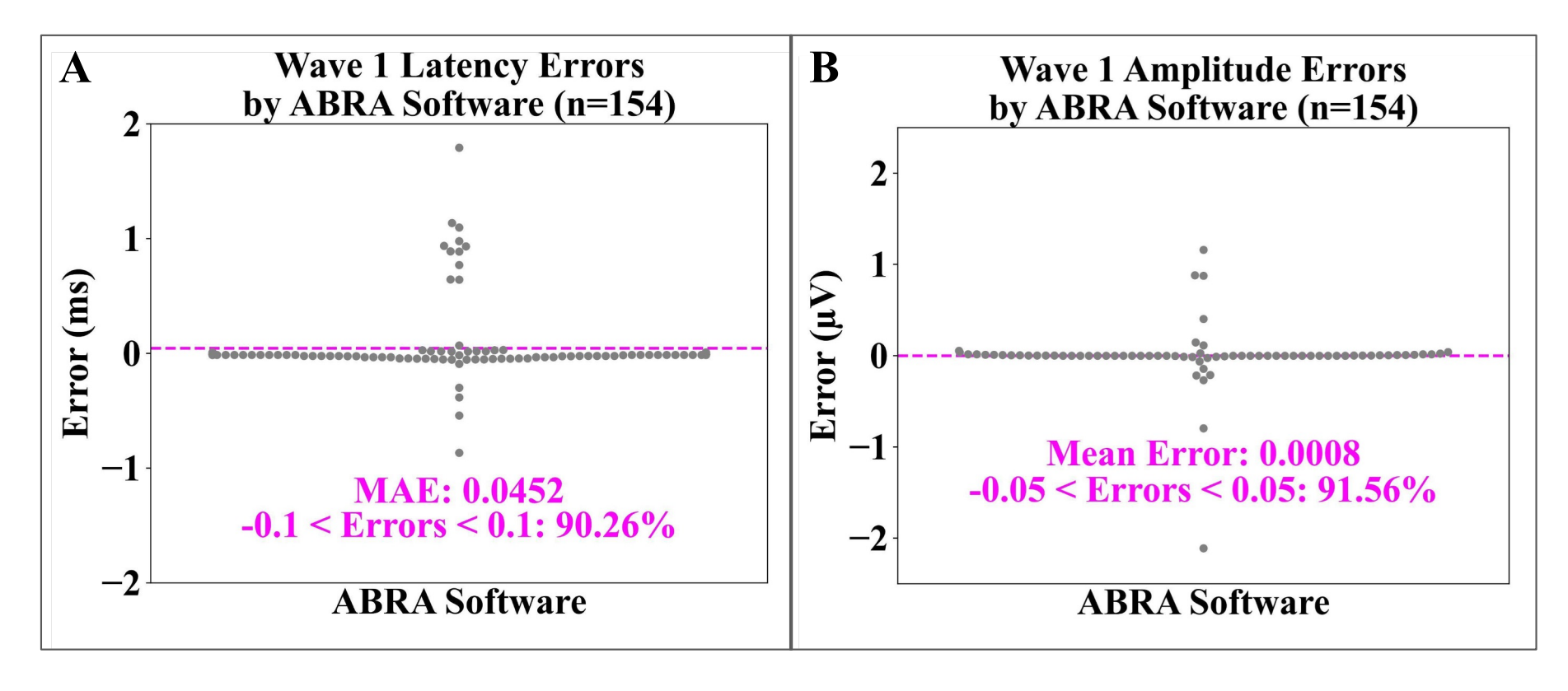
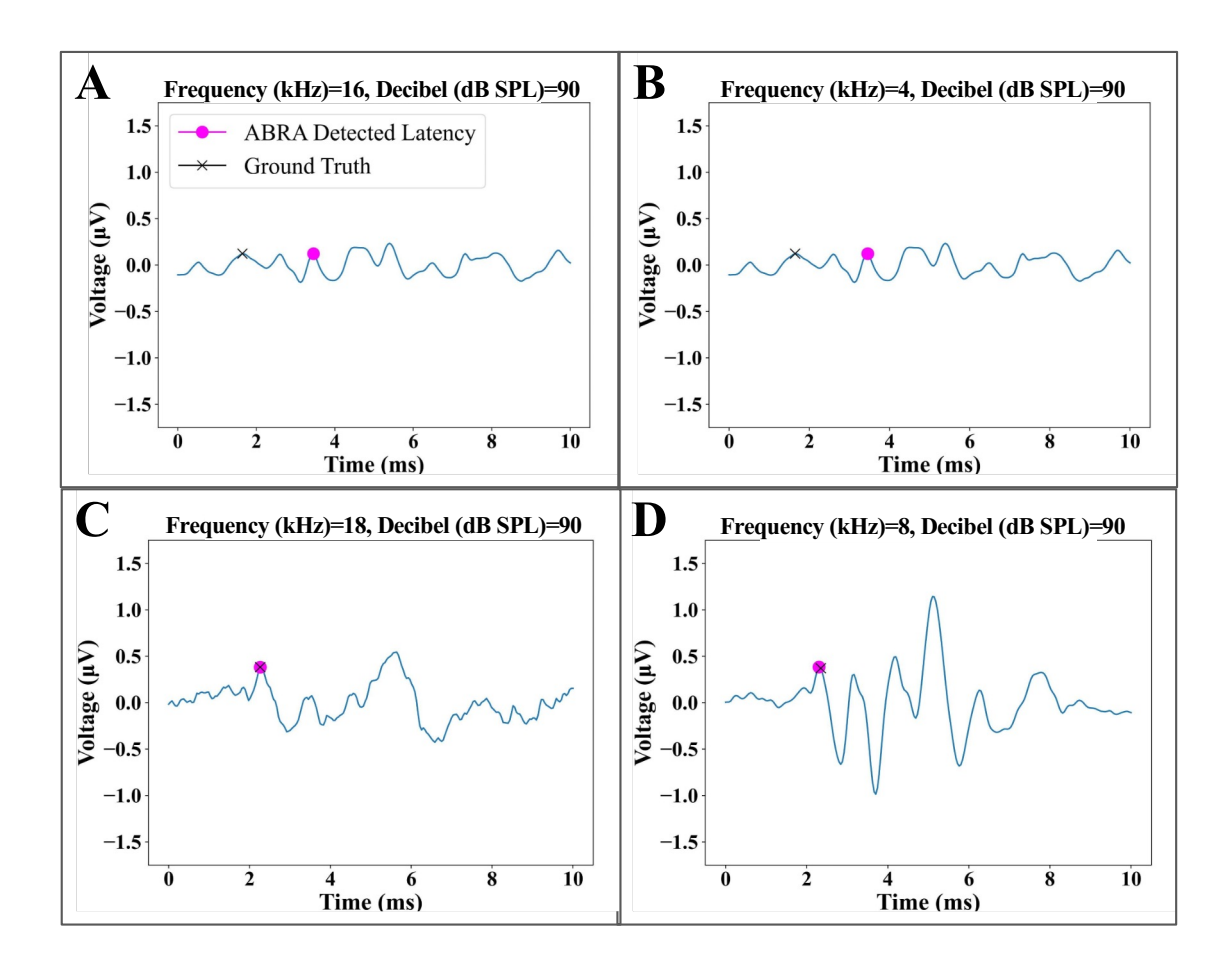
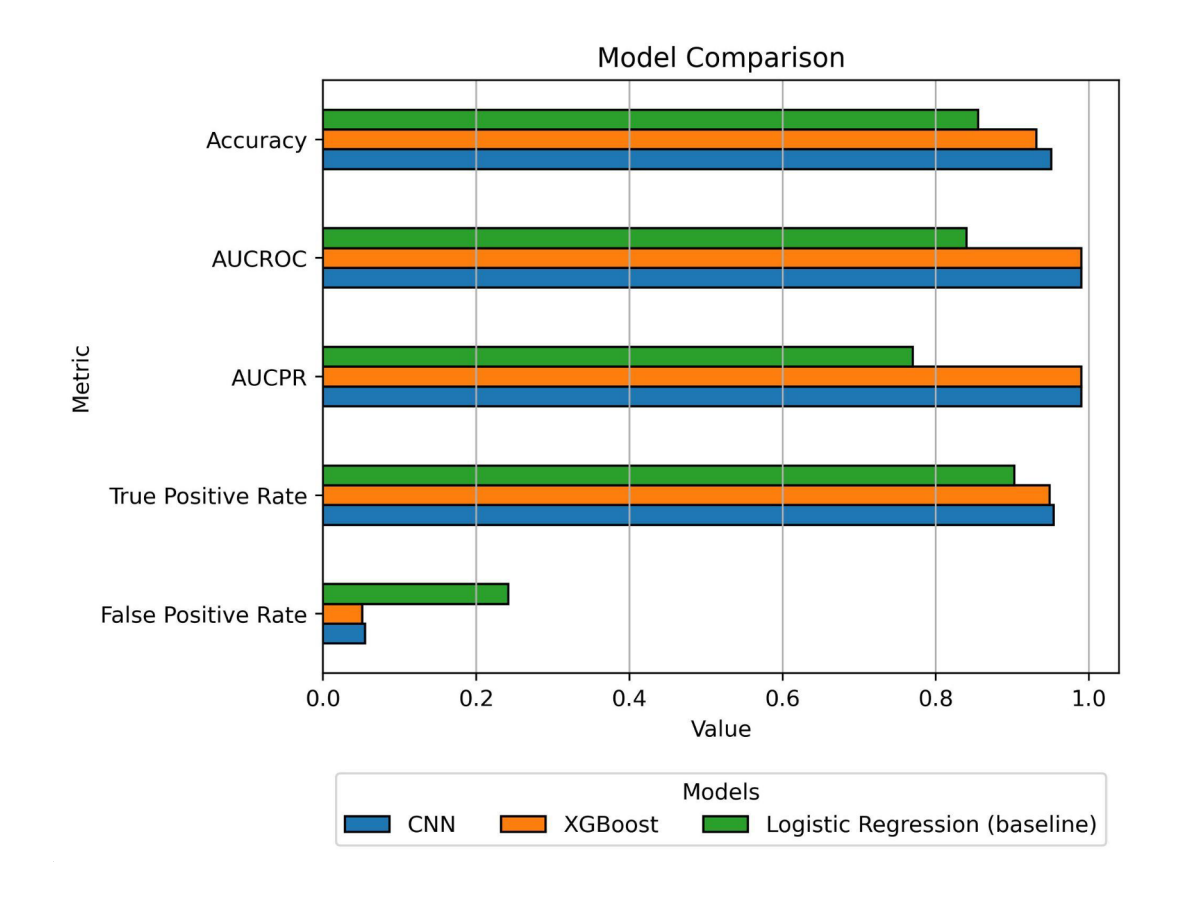


Figure 6: Swarmplots displaying spreads of error for detected Wave 1 Latency (A) and Amplitude (B) vs. ground truth for each software. Testing failed to find evidence that mean absolute errors were significantly greater than zero for both Wave 1 Latency and Amplitude estimates. 90.26% of all ABRA-generated estimates of Wave 1 Latency were within 0.1ms of the corresponding true human-labeled latency; 91.56% of all ABRA-generated Wave 1 amplitude were within 0.05  $\mu$ V of the corresponding true human-labeled peak amplitude.



**Figure 7: Examples of error cases in peak detection.** (A) example of multiple peaks that may be identified as Wave 1 by different softwares and different sets of eyes. (B) ABRA may identify the incorrect peak. (C) and (D) are examples of ABR waveforms with larger signal to noise ratios for which ABRA matches the ground truth.



**Figure 8: Comparative Analysis of Machine Learning Models.** Horizontal bar chart illustrating the performance of three machine learning models: Convolutional Neural Network (CNN), XGBoost, and Logistic Regression (baseline). The metrics used for comparison are Accuracy, True Positive Rate, False Positive Rate, Area Under the Receiver Operating Characteristic Curve (AUCROC), and Area Under the Precision-Recall Curve (AUCPR). The CNN model exhibits the highest accuracy, while the Logistic Regression model serves as the baseline for comparison

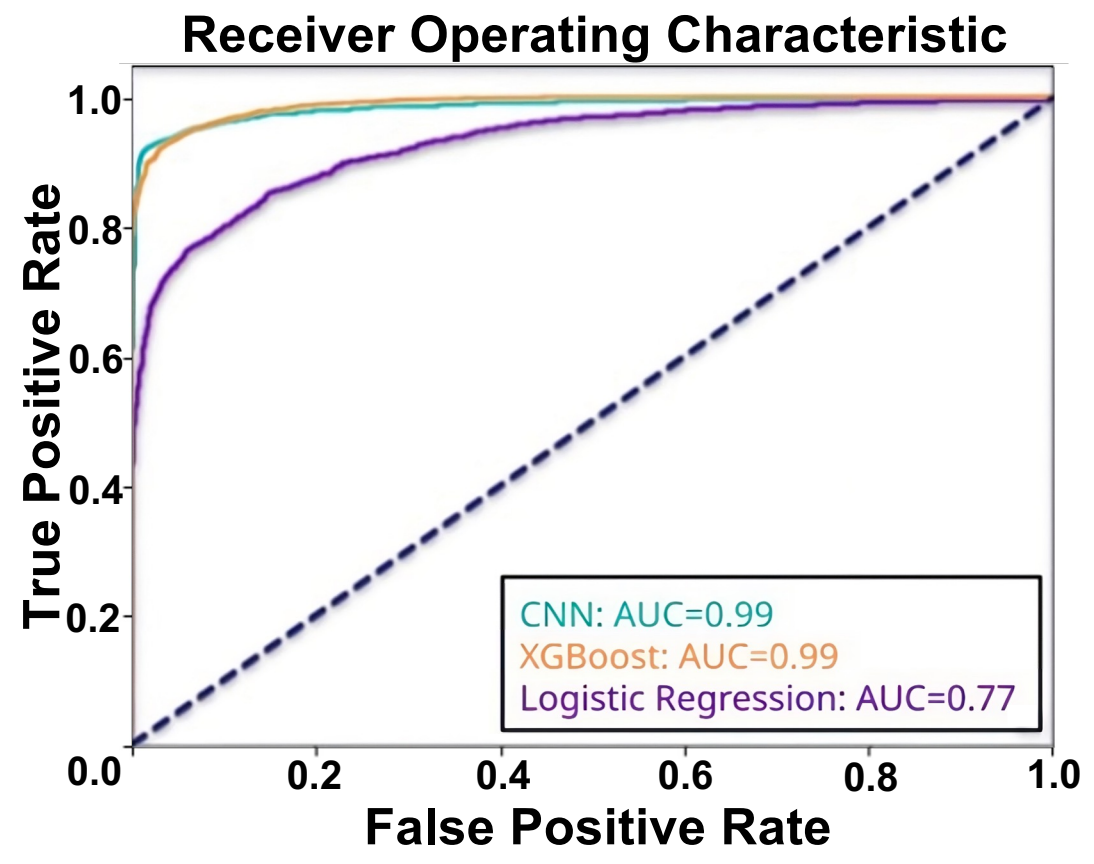


Figure 9: Receiver Operating Characteristic (ROC) Curves and Areas Under Curves (AUC) for Convolutional Neural Network (CNN), XGBoost, and Logistic Regression Classifiers. A ROC curve demonstrates the performance of an ABR classifier at all classification thresholds. The area under the ROC curve represents the ABR classifier's overall ability to distinguish between ABR responses that are above the hearing threshold and those that are not under varying model settings. The ROC curves for the CNN and XGBoost classifiers are nearly identical, while that of the Logistic Regression classifier suggests relatively inferior performance.

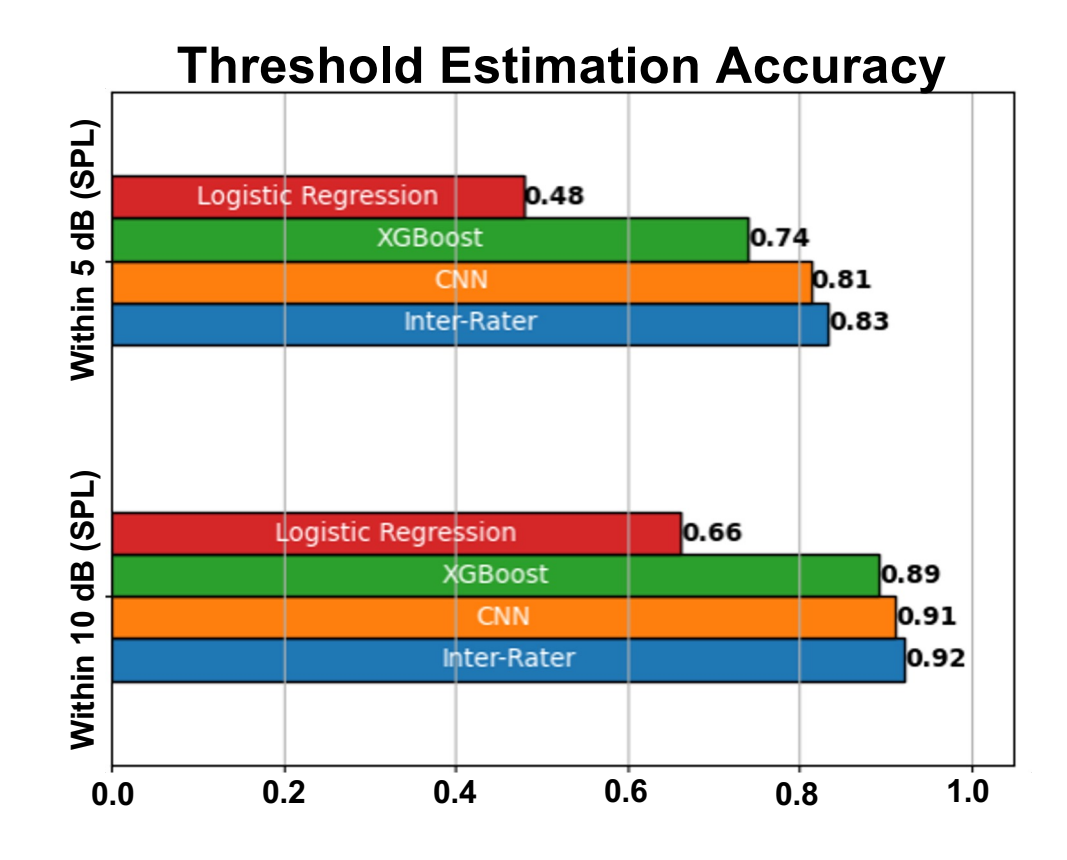


Figure 10: Threshold Estimation Metrics for Machine Learning Models and Human Expert Inter-Rater Comparison. Bar chart comparing the performance of three machine learning models: Convolutional Neural Network (CNN), XGBoost, and Logistic Regression, as well as an Inter-Rater comparison based on their ability to estimate thresholds within 5dB and 10dB. The Inter-Rater comparison was conducted by comparing 100 threshold estimates of two experts. The CNN and XGBoost models demonstrate superior performance compared to the Logistic Regression model, with the CNN outperforming XGBoost at higher levels of precision. The Inter-Rater comparison provides a benchmark for human expert performance in the task.